This research was originally published in The Journal of Biological Chemistry.
Jose R. Couceiro, Rodrigo Gallardo, Frederik De Smet, Greet De Baets, Pieter Baatsen, Wim Annaert, Kenny Roose, Xavier Saelens, Joost Schymkowitz, and Frederic Rousseau
Sequence-dependent internalisation of aggregating peptides.
J. Biol. Chem First Published on November 12, 2014,doi:10.1074/jbc.M114.586636. © the American Society for Biochemistry and Molecular Biology

Sequence-dependent internalisation of aggregating peptides

José R. Couceiro[1,2], Rodrigo Gallardo[1,2], Frederik De Smet[1,2], Greet De Baets[1,2], Pieter Baatsen[3,4], Wim Annaert[5], Kenny Roose[6,7], Xavier Saelens[6,7], Joost Schymkowitz[1,2] and Frederic Rousseau[1,2]

[1] Switch Laboratory, VIB, Leuven, Belgium

[2] Switch Laboratory, Department of Cellular and Molecular Medicine, KULeuven, Belgium

[3]Electron microscopy facility (EMoNe), KU Leuven Centre for Human Genetics, Belgium

[4] VIB BIO Imaging Core, VIB, Leuven, Belgium

[5]Laboratory for Membrane Trafficking, KU Leuven and VIB-Centre for the Biology of Disease, Leuven, Belgium

[6]VIB Inflammation Research Center, 9052 Ghent, Belgium

[7]Department of Biomedical Molecular Biology, Ghent University, 9052 Ghent, Belgium

*Running title: Size dependent uptake of peptide aggregates

To whom correspondence should be addressed: Frederic Rousseau, Switch Laboratory, Department of Cellular and Molecular Medicine, Gasthuisberg Campus O&N1, Herestraat 49 bus 802, B-3000 Leuven, Belgium. Tel.: (+32) 16 3 72572; Fax: (+32) 16 3 72571; E-mail: frederic.rousseau@switch.vib-kuleuven.be

Keywords: Protein aggregation; Prionoid; Cellular Uptake; Chaperones; Endocytosis

Background: Prionoid propagation requires cells internalization of aggregated polypeptides.

Results: Aggregates of different sequence are internalized through different endocytic pathways.

Only phagocytozed aggregates (>1 μm) elicit an HSF1-dependent proteostatic response.

Conclusion: Proteostatic response upon aggregate internalization differs markedly depending on the sequence.

Significance: The characterisation of mechanisms of cell penetration is fundamental for the understanding of aggregate transmission in disease.

ABSTRACT

Recently a number of aggregation disease polypeptides have been shown to spread from cell to cell thereby displaying prionoid behaviour. Studying aggregate internalisation however is often hampered by the complex kinetics of the aggregation process resulting in the concomitant uptake of aggregates of different sizes by competing mechanisms, which makes it difficult to isolate pathway-specific responses to aggregates. We designed synthetic aggregating peptides bearing different aggregation propensities with the aim of producing modes of uptake that are sufficiently distinct to differentially analyse the cellular response to internalization. We found that small acidic aggregates (≤500 nm diameter) were taken up by non-specific endocytosis as part of the fluid phase and travelled through the endosomal compartment to lysosomes. By contrast, basic aggregates bigger (>1 μm) were taken up through a mechanism dependent of cytoskeletal reorganization and membrane remodelling with the morphological hallmarks of phagocytosis. Importantly, the properties of these aggregates not only determined the mechanism of internalization but also the involvement of the proteostatic machinery (the assembly of interconnected networks that control the biogenesis, folding, trafficking and degradation of proteins) in the process: while the internalization of small acidic aggregates is HSF1 independent, the uptake of larger basic aggregates was HSF1 dependent requiring Hsp70. Our results show that the biophysical properties of aggregates determine both their mechanism of internalisation and proteostatic response. It remains to be seen whether these differences in cellular response contribute to the particular role of specific aggregated proteins in disease.

Recently it has been demonstrated that several disease-associated aggregates, including human (1–3) and yeast prions (4), Aβ (5), Tau (6), α-Synuclein (7), SOD1 (8) and PolyQ (9) can cross cellular membranes and spread aggregation from cell to cell (10). This has led to the notion that all these proteins potentially possess a certain degree of prionoid behaviour (8, 11, 12). Despite these reports the mechanism by which this process takes place remains obscure as the transmission of a protein or aggregate from the cytosol of one cell to the cytosol of a neighbouring cell requires the crossing of both cellular membranes. The existence of cell membrane translocation mechanisms has been proposed for some amyloids, such as nanotubules for prions (3) or membrane diffusion by an unknown mechanism for Aβ40 (13, 14) and α-Synuclein (15), although it is widely accepted nowadays that aggregate transmission can also occur through a combination of exocytosis, endocytosis and endosomal escape (16).

In accordance with this hypothesis, several mechanisms of endocytosis and exocytosis have been postulated for the most common amyloids. Exocytosis by conventional exosomes, as the result of the fusion of multivesicular bodies with the plasma membrane, has been reported for monomeric Aβ (17), α-Synuclein (18–20), PrpSc (2, 21), and Tau (22) in neuroblastoma cell lines. Other unconventional exocytosis mechanisms have been described for PrP (23) and α-Synuclein (19). Endocytosis of monomeric Aβ (13, 14, 24–26) and α-Synuclein (15, 27–29) and endocytosis of the fibrillar and oligomeric states of some amyloids have also been reported. For instance, fibrilar Aβ can be cleared from the medium by microglia and astroglia (30–32) while oligomeric Aβ can be taken up by neuroblastoma SH-SY5Y cells (33). The internalization of PrpSc aggregates has been reported in murine and human neuroblastoma cell lines and mouse fibroblasts, whereby heparan sulphates and lipid rafts turned out to be involved (1, 34–37). SOD1 aggregates are internalized by macropinocytosis by N2a cells, a neuroblastoma cell line (8), while Tau aggregates were taken up by HEK-293 cells and neuroblastoma cell lines (6, 38, 39). Currently it is not known whether different amyloids share common pathways of internalization. Besides, different pathways of internalization have been

described for the monomeric and fibrillar forms of α-Synuclein (15) and Aβ (13, 32), demonstrating that the aggregation status could also determine different routes of internalization. Finally, interaction of the native protein with natural partners could also determine specific handling by a specific subset of cells, as occurs during the intracellular production of Aβ (40, 41).

Here our aim is to investigate whether the biophysical properties of an aggregating polypeptide sequence affects the way in which it is recognized and processed by the cell. As several competing uptake mechanisms have been previously described our objective here was therefore to design synthetic aggregating peptides with a strong bias towards a particular mode of uptake, which would illustrate how biophysical properties affect uptake and would allow to investigate pathway-specific cellular responses to aggregates. It is accepted that a size threshold determines the choice of the endocytic pathway that will be used for the uptake of different extracellular bodies. While particles below 0.5 µm in diameter could be internalized through clathrin, caveolin or general pinocytosis, particles of a bigger diameter will require the activation of a macropinocytic or phagocytic process (42). To this purpose, we have compared the internalization of two synthetic peptides with different aggregation propensities resulting in aggregate particles of different sizes. We found that aggregates of both peptides are efficiently internalized by non-specialist cells in culture. Further aggregate size not only determine the mechanism of uptake but also modulate the involvement of the proteostasis machinery in the process. While large aggregates with a diameter bigger than 0.5 µm diameter were taken up by phagocytosis in a Heat Shock Factor 1 (HSF1) dependent manner, smaller aggregates were internalized through fluid phase endocytosis in an HSF1 independent manner.

Our work demonstrates that aggregate uptake is an inherent activity of mammalian cells. It also shows that biophysical parameters that affect the aggregation propensity and particle size determine the mode of uptake as well as the proteostatic response to aggregates: whereas larger aggregates are detected by the proteostatic machinery and actively internalized, smaller aggregates remain largely undetected and enter the cell in an unspecific manner.

EXPERIMENTAL PROCEDURES

Peptides and Reagents. Peptides PepL (sequence: RPILTIITLE RGSRRPILTI ITLE, Tango score: 1273.17), PepS (sequence: DMISYAGMDP PDMISYAGMD, Tango score: 10.44), Inf12 (sequence: RLIQLIVSRP PRLIQLIVSR, Tango score: 532.08) and Inf36 (sequence: RGVSILNLRP PRGVSILNLR, Tango score: 29.36) were custom synthesized by JPT at a purity >95% as determined by HPLC. Lyophilised peptide powder was resuspended in DMSO to 2 mM concentration. This DMSO stock solution was diluted to working solutions in PBS or cell culture medium ranging from 2 to 20 µM as indicated in each experiment. DLS analysis was performed in a DynaPro Plate Reader II (Wyatt Technology) equipped with a 830 nm wavelength laser and Dynamics software (Wyatt Technology) was used to analyse the data. The antibody against the extracellular region of membrane Hsp70, cmHSP70.1, was a kind donation of Prof. Dr. Gabriele Multhoff. The inhibitors dynasore hydrate, EIPA (5-(N-Ethyl-N-isopropyl)amiloride), cytochalasin D, MβCD (Methyl-β-cyclodextrin), mevinolin, rapamycin and chlorpromazine hydrochloride were purchased from Sigma-Aldrich, KRIBB11 was obtained from Merck Chemicals, VER155008 from Tocris Bioscience and geldanamycin from Invivogen. Dextran 10000 MW conjugated to Texas Red was purchased from Life Technologies. Purified Hsp70 was obtained from ENZO life sciences. Before cell culture incubations, storage solution was substituted by PBS in a Zeba Spin Desalting Column 7K (Thermo Scientific)**.**

Cell culture, transfections and peptide incubations. HEK-293 cell line was cultured in DMEM supplemented with 10% (v/v) FCS (Gibco), penicillin (100 U/ml) and streptomycin (100 U/ml). Proliferating cell cultures were maintained in a 5% CO2 humidified incubator at 37°C. Transfections were performed with FuGENE HD (Promega) according to the manufacturer recommendations. Cellular expression of RFP fusions of proteins Rab5, Rab7 and Lamp1 was achieved by the use of baculovirus based BacMam 2.0 probes (Life Technologies). GFP-LC3 expression was performed by transduction of cells with Lentibrite Lentiviral Biosensor following the manufacturer recommendations (Merck Milipore). For peptide

treatments of culture cells, 2 mM peptide stock solutions in DMSO were diluted to a 20 µM concentration in serum-free DMEM-F12 medium (Gibco) to allow the formation of aggregates before addition to the cells. Cells in culture were always at 90% confluency when peptide was added to the medium. For 20 µM incubations, cells were incubated for 1 hour in the peptide solution and then washed and incubated for different periods of time in complete cell culture medium. For 5 µM and 2 µM incubations, 20 µM peptide solutions were added to the cell culture medium as 4x or 10x concentrates respectively and no further wash steps were performed unless otherwise indicated.

Immunofluorescence staining, in vivo confocal and time lapse confocal. Cell imaging was performed *in vivo* unless otherwise indicated using an inverted microscope (Nikon Eclipse TE2000-S) equipped with a Confocal Microscopy Imaging System (Nikon Eclipse C1). For time lapse experiments, a Nikon A1R Eclipse Ti was used. cmHsp70.1 staining was performed *in vivo* as follows: after overnight incubation in complete cell culture medium containing 5 µM peptide or 10 µM geldanamycin, cells were first blocked in a solution of 20% goat serum and 0.2% tween-20 in PBS for 10 min and incubated right after for 1h in 1:100 or 1:1000 antibody dilutions in PBS. Cells were then washed in PBS three times before being fixed in 4% paraformaldehyde in PBS. After fixation, cells were washed 3 times in PBS and mounted in ProLong Gold Antifade Reagent with DAPI (Life Technologies). High content analysis was performed *in vivo* in an IN Cell Analyzer 2000 (GE Healthcare). The software IN Cell Developer was used for the quantification of the different structures. Internalised aggregates were differentiated from extracellular membrane-attached aggregates by means of their higher fluorescence intensity. Small peripheral endolysosomes were distinguished by their smaller size.

Transmission Electron Microscopy. For peptide aggregate solution analysis: 20 µM peptide suspensions in PBS were adhered onto carbon-coated copper grids and stained in a solution of 2% Uranyl acetate for 5 min. After 5 rounds of washing in ultrapure water, grids were analysed in a JEM-1400 transmission electron microscope. Cell samples were grown on Aclar and incubated with peptide as described above. At given time points they were fixed overnight at 4˚C in 0.1 M sodium-cacodylate buffer containing 2.5% glutaraldehyde. After washing, they were fixed additionally for 2 hours at 4˚C in 1% osmium tetroxide, rinsed with distilled water and dehydrated through a graded ethanol series. During the dehydration steps they were stained in 3% uranyl acetate/70% ethanol for 30 min at 4˚C. After the last step in 100% ethanol, samples were washed in Propylene Oxide and embedded in Epoxy resin (Epoxy-Embedding Kit, Fluke Analytical). After polymerization, 50 nm slices were obtained and transferred to carbon-coated copper grids. Grids were subsequently post-stained for 10 min in 3% uranyl acetate/water and for 5 min in a lead citrate solution (Reynolds' formulation). After extensive washes in water, grids were air-dried and analysed in a JEM-1400 transmission electron microscope.

Microarrays. Cells were incubated with the different peptides as indicated above. After 24 hours of incubation, total RNAs were extracted using RNeasy Mini Kit (QIAgen). RNA concentration and purity were determined spectrophotometrically using the Nanodrop 2000 (Thermo Scientific) and RNA integrity was assessed using a Bioanalyser 2100 (Agilent, Santa Clara, CA, USA). Per sample, an amount of 100 ng of total RNA spiked with bacterial RNA transcript positive controls (Affymetrix) was amplified and labelled using the GeneChip 3' IVT express kit (Affymetrix). All steps were carried out according to the manufacturer's protocol (Affymetrix). A mixture of purified and fragmented biotinylated RNA and hybridisation controls (Affymetrix) was hybridised on Affymetrix GeneChip® PrimeView™ Human Gene Expression Arrays followed by staining and washing in a GeneChip® fluidics station 450 (Affymetrix) according to the manufacturer's procedures. To assess the raw probe signal intensities, chips were scanned using a GeneChip® scanner 3000 (Affymetrix). Raw data were processed all together with the RMA algorithm (43) and subsequently subjected to a two-factor ANOVA (analysis of variance)**.**

RESULTS

Synthetic aggregation prone peptides with low and high aggregation propensities form

aggregate pools of largely non-overlapping size distributions in vitro**.** Most aggregating peptides and proteins form aggregates ranging from soluble oligomers to large insoluble inclusions. Moreover the size distribution of these aggregates evolves over time, which makes it difficult to isolate aggregates of a specific size-range in solution. In order to partially circumvent this difficulty, we used TANGO (44), an algorithm to predict protein aggregation, to select two peptide sequences with either low or high aggregation propensities with the aim of generating two aggregate populations with non-overlapping (or minimally overlapping) size-distributions over sufficient time to study the cellular internalization of these peptides.

A peptide with low aggregation propensity and negative charge, referred to as PepS (for small, amino acid sequence DMISYAGMDPPDMISYAGMD, Tango score: 10,44, pI=3.3) (Table 1), was derived from the vascular-endothelial growth factor receptor 2 (VEGFR2) protein sequence. When put in solution in PBS at a concentration of 20 µM, amorphous aggregates of different sizes were observed by electron and confocal microscopy (Fig. 1A). Although particles above 1µm were occasionally observed, confocal images and DLS indicated that most of the peptide molecules were in a monomeric or oligomeric status (0.5 nm diameter) or in aggregates with a size distribution around 100 nm (Fig.1B). A prolonged incubation for over a month at 37˚C with shaking at 1000 rpm did not increase the maximum size of the aggregates, although the amount of low molecular weight aggregates decreased in favour of the formation of aggregates of an approximate diameter of 500 nm (data not shown).

The sequence of the highly aggregating positively charged peptide, referred to as PepL (for large, amino acid sequence RPILTIITLERGSRRPILTIITLE, Tango score: 1280, pI=11.5) (Table 1), consists of a tandem repeat of an aggregation-prone sequence of the p53 DNA binding domain (45). Analysis by electron and confocal microscopy of a 20 µM solution of this peptide in PBS showed, as for PepS, a heterogeneous population of amorphous aggregates of different sizes but, contrary to PepS, confocal analysis of PepL solutions showed an enrichement in aggregates that typically exceeded 1 µm diameter (Fig. 1A) although a population of aggregates of smaller size was also present (Fig. 1A). DLS analysis confirmed that this solutions are mainly composed of aggregates well over 1 µm in diameter (Fig. 1B).

We therefore managed to select two aggregating peptide sequences displaying very different charge and size-distributions. Importantly, although the size distributions of PepS and PepL evolved over time, they remain distinct with PepS peptides never exceeding a maximum size of 500 nm while PepL immediately formed aggregates larger than 1 µm.

PepL aggregates are fragmented on the cell surface prior to internalisation. PepL was added to the culture medium of HEK-293 cells at a concentration of 20 µM. After 1 hour incubation, association of the aggregates to the cell membrane could be detected after a medium change to wash away unbound aggregates (Fig. 2A). Time-lapse microscopy revealed that this association was not just deposition of the aggregates on the cell membrane, but rather a dynamic interaction between peptide aggregates and the cell membrane. Two main processes were observed in this interaction. On the one hand, the biggest aggregate particles were fragmented to smaller particles (Fig. 2A, upper panels, arrows, Video 1). On the other hand, aggregates were able to move along cells and even migrate from them to neighbouring cells (Fig. 2A, upper panels, arrows). In some cases, aggregates contacting the periphery of a cell moved towards perinuclear regions of it where they were engulfed (Fig. 2A, lower panels, arrowhead, Video 2). Confocal analysis in living cells confirmed that aggregate internalization was associated with fragmentation of large aggregates into smaller aggregates, rather than disaggregation into monomeric/single peptides. To visualize this we first prepared two separate solutions of aggregates, each labelled with a different fluorophore (Dylight#488 and Dylight#550) and subsequently mixed these together immediately before adding them to the cells. Upon mixing, both aggregates further matured into heterogeneous aggregates containing both labels (Fig. 2B, 1h). Rather than forming vesicles containing these heterogeneous aggregates, the internalized aggregates were generally labelled with only one of the fluorophores. Thus upon contact with the cell membrane aggregates are broken down to smaller units corresponding to premixing

aggregate nuclei rather than being disaggregated (Fig. 2B, 8h).

PepL is internalized by phagocytic processes. The irregular morphology of the vesicles formed after internalization of the aggregates suggests phagocytic internalization. Following the process by TEM further corroborated this idea, showing contacts between aggregates and membrane, protrusions reaching over the surface of the aggregates and final engulfment (Fig. 2B, left panels). To corroborate this, a set of inhibitors of different endocytic pathways was used to better define the pathway implicated in aggregate internalization. To this end, high content analysis was performed, quantifying an average of 2000 cells per sample for the presence and number of endocytic particles, which were discerned depending on their different size and fluorescence intensity (see Experimental Procedures). In our assay conditions, only a percentage of cells ranging from 10 to 40% takes up an average of one aggregate per cell. So the percentage of cells containing one aggregate in the population, rather than the number of aggregates internalized per cell, was used as measure of peptide uptake. This percentage was reduced by inhibitors like dynasore (inhibitor of dynamin-driven endocytosis), cytochalasin D (inhibitor of actin cytoskeleton reorganization), EIPA (inhibitor of the Na^+/H^+ pump) and acute treatment of the cells with MβCD (Methyl-β-CycloDextrin, a membrane cholesterol depletor) followed by chronic inhibition of cholesterol synthesis with mevanolin (Fig. 2C). All this inhibitors, although not specific for phagocytosis, have been previously described as phagocytosis inhibitors (46–49). On the other hand, uptake of the aggregates was not inhibited by a clathrin mediated endocytosis inhibitor such as chlorpromazine (Fig. 2C). Taking together the morphological and pharmacological data, the internalization of large aggregates formed by PepL is most likely due to phagocytic uptake.

PepL disaggregation in endosomes is associated with endosomal swelling. Once internalized, the particles formed vesicles of irregular size with increased fluorescence levels (Fig. 2B, 8h). As the internalization progressed the endosomal vesicles expanded and increased their fluorescence intensity, probably due to fluorophore dequenching. Both facts suggest that peptide disaggregation into soluble monomeric or oligomeric peptides occurs in this vesicles (Fig. 2, 24 h). The resulting enlarged endosomes are non-homogenous. Their fluorescence intensity depicts an aggregated part of irregular shape at one pole surrounded by a rounded envelope of soluble material (Fig. 2B, 24h). TEM analysis confirms this arrangement as the micrographs clearly show aggregated material at one pole of the vesicle surrounded by smaller soluble peptide particles, which is again indicative of disaggregation activity (Fig. 2, 24h). Interestingly, these enlarged endosomal vesicles were particularly sensitive to photodisruption, as illumination with the confocal laser made the vesicles burst in a typically two-phases event. In a first movement, illumination resulted in membrane contraction probably due to photo-oxidative membrane damage (Fig. 3A, panels 1-3, Video 3). This was then followed by vesicle dilatation until a final burst liberated its contents into the cytosol (Fig. 3A, panels 4-6, Video 3). These enlarged endosomal vesicles could also be observed by bright field microscopy with non-labelled peptide, excluding that vesicle swelling is a fluorophore-associated artefact (Fig. 3B, panel 1, arrows). The structure remained morphologically identical after formaldehyde fixation when observed by bright field microscopy (Fig. 3B, panel 2, arrows). However after chemical fixation and permeabilization with detergents only the aggregated part of the enlarged endosomal vesicles remained, seeming like cytoplasmic inclusions of irregular shape by fluorescent microscopy (Fig. 3B, panel 3). Only under conditions of high background autofluorescence, e.g. when using glutaraldehyde fixation, the structure of the enlarged vesicle was fully depicted, as the empty vesicular part appeared black in contrast to the surrounding fixed cellular cytoplasmic content (Fig. 3B, panel 4, arrows).

PepL aggregates are trafficked into the endolysosomal pathway. To characterize the vesicular trafficking of the aggregates, HEK-293 cells were transfected with expression vectors of several fluorescently labelled endocytosis markers before being exposed to the aggregates. We observed that ruffled vesicles and enlarged endosomal vesicles were positive for Rab7 staining and weakly positive for Rab5 staining (Fig. 4A, left panels), indicating that these compartments acquire late endosome properties rather quickly. Both ruffled and enlarged vesicles

also stained for the lysosomal marker Lamp1, indicating that fusion with lysosomes or late endosomes already took place (Fig. 4A, left bottom panels). After 8 hours of incubation, relatively small peripheral rounded vesicles containing the peptide were detected in the cells. These vesicles did not co-localize with the marker Rab5, but they did with markers Rab7 and Lamp1 (Fig. 4A, right panels). Because the culture medium was refreshed after the first hour of incubation, these vesicles are more likely due to the distribution of material contained in ruffled and enlarged vesicles into peripheral endolysosomes, rather than to fluid phase endocytosis of soluble peptide still present in the extracellular solution.

Despite Rab5 being just weakly visible in the membranes of the vesicles, its function is necessary for the progression of the peptides through the endosomal compartment. In fact, the expression of a constitutively active mutant of this protein ($Rab5^{Q79L}$) prevented the distribution of the peptide to the peripheral endolysosomes (Fig. 4B).

PepS is trafficked to the endolysosomal pathway by fluid phase endocytosis. The pathway of internalization of peptide PepS was different from that of PepL from both a morphological and a functional perspective. First, contrary to PepL, confocal imaging did not detect any association of PepS with the cell membrane (Fig. 5A). Further, the uptake of PepS was similar in time and morphology to the internalization of a fluid phase marker (TexasRed-Dextran10) suggesting a mechanism of fluid phase endocytosis (Fig. 5A). Thus, the internalization of this peptide takes place through the formation of vesicles of a diameter ranging from 0.5 μm to 1 μm that increase progressively in fluorescence intensity over time, indicating peptide accumulation (Fig. 5A). The effect of specific endocytic inhibitors was also in agreement with fluid phase endocytosis as only partial inhibition of this process could be achieved. Through high content microscopy analysis, this decrease in the uptake can be quantified as a reduction of the number of detectable intracellular vesicles. Dynasore is the inhibitor with the biggest impact, reducing the intracellular number of vesicles to 50% in treated cells (Fig. 5B). The macropinocytosis inhibitor EIPA has a marginal impact on the number of vesicles detected indicating that most of the peptide is internalized through other pathways. Inhibition of the cytoskeleton dynamics by cytochalasin D showed a decrease in the number of vesicles of about 25% (Fig. 5B). This could be due to a decrease in the phagocytosis or macropinocytosis of the particles of bigger size present in the solution. Finally, chlorpromazine showed an increase in peptide uptake both in number and size of the vesicles (Fig. 5B), which suggests a compensation effect on endocytic uptake through clathrin independent endocytosis, such as pinocytosis and macropinocytosis. Overall, the partial and compensatory effects caused by the inhibitors indicate that the peptide was internalized as bulk in the fluid phase during constitutive endocytosis and not as a result of specific membrane recognition, signalling and uptake.

The use of the endocytosis markers described earlier showed that vesicles that accumulate peptide were positive for Rab7 and Lamp1 (Fig. 5C). Rab5 positive vesicles were spotted as well, more abundantly at short incubation times (Fig. 5C). Overexpression of the constitutively active mutant $Rab5^{Q79L}$ induced an arrest of the internalized PepS in early endosomes (Fig. 5C), as shown before for PepL. Together this indicates that both PepS and PepL trafficking converge towards endolysosomal pathways.

PepL and PepS differ in several biophysical parameters, such as pI, hydrophobicity and aggregation propensity, which can modify their mechanism of interaction with membranes. It has been described that electrostatic interactions play an important role in protein-membrane interactions, and therefore the difference in net charge of the peptides could influence the difference in uptake mechanism. To rule out this possibility we studied the cellular uptake of another set of peptides that have the same charge and similar mean hydrophobicity but only differ in their aggregation propensity. These peptides, called Inf12 and Inf36, are derived from aggregating stretches found in the basic polymerases 1 and 2 (PB1 and PB2) of the Influenza A virus (Inf36 RGVSILNLRP PRGVSILNLR and Inf12 RLIQLIVSRP PRLIQLIVSR, respectively) (Table 1). Having very different tango scores (29 and 532, respectively) they form small aggregates (79% of particles in solution are about 200 nm) and larger aggregates (64% of aggregates around 10 μm)

respectively (Fig. 1). Corroborating our previous results, the highly aggregating peptide Inf12 was internalized through the formation of large cytosolic inclusions as observed for peptide PepL (Fig. 6, upper panels, arrows). On the other hand, Inf36, the least aggregating peptide, was taken up through a mechanism resembling fluid phase endocytosis (Fig. 6, lower panels), with gradual accumulation of peptide over time in relatively small intracellular compartments, as observed for PepS. Although this additional experiment does not resolve the particular biophysical factors determining aggregate uptake these results suggest that aggregate size plays an important modulating role on the mode of aggregate uptake by cells.

PepL but not PepS internalisation requires Hsp70 and is HSF1 dependent. As phagocytosis is a specific and active process, our results suggested that extracellular aggregates were specifically recognized as cargo and internalized upon intracellular signalling. We therefore analysed the role of the protein quality control system (PQC) during aggregate internalisation. The PQC consists of chaperones, which assist protein folding and trafficking, and the degradation machinery, comprised mainly of the proteasome and autophagy systems working independently or in collaboration with ubiquitin-ligases (50–52). Besides, dedicated transcription factors promote the expression of the necessary PQC components upon proteotoxic stimuli. Among these transcription factors, the Heat Shock Factor 1 (HSF1) has a prominent role (53).

HEK-293 cells were treated before and during incubation in medium containing aggregating peptides with inhibitors of the chaperones Hsp70 (VER155008) and Hsp90 (geldanamycin), a specific inhibitor of HSF1 (KRIBB11) and an autophagy stimulator (rapamycin). Treatment with VER155008 decreased the number of cells containing internalised PepL to 20% with respect to the untreated controls, indicating prominent role for Hsp70 in PepL aggregate uptake (Fig. 7A). Consistent with the above result, inhibition of HSF1 produced a similar inhibition pattern (Fig. 7A), showing that the uptake of large extracellular aggregates requires a proteostatic response. Contrary to PepL, the uptake of PepS was not affected by VER155008 or KRIBB11 since the use of these inhibitors didn't decrease the amount of peptide being internalised by cells (Fig. 7A). This indicates that fluid phase endocytosis of small aggregates is unspecific and HSF1 independent. As a control for the specificity of the Hsp70 inhibitors in aggregate uptake, phagocytosis of polystyrene beads of 3 μm of diameter was tested in the presence of the aforementioned inhibitors. Bead uptake was efficiently blocked by endocytosis inhibitors such as cytochalasin D but, on the contrary, none of the PQC inhibitors tested, including KRIBB11 and VER155008, had negative effects on bead internalisation (Fig. 7A), which argues for a specific role of Hsp70 in the uptake or endosomal trafficking of extracellular aggregates rather than a general role in phagocytosis or macropinocytosis of any type of particle.

Geldanamycin treatment did not reduce the number of cells internalising PepL aggregates, nor the number of internalised aggregates per cell (not shown), although the number of peripheral endolysosomes per cell decreased (Fig. 7A). Since the number of cells with internalised aggregates is the same as in untreated cells, the reduction in the number of endolysosomes can only be explained by a role of Hsp90 in endosomal trafficking between early endosomes and lysosomes (54). Geldanamycin also affected the endosomal trafficking of PepS. In this case, we observed an increase in the average endosome size associated with a 40% decrease in the number of peptide-containing vesicles (Fig. 7A).

Finally, autophagy has been implicated in the degradation of intracellular aggregates through chaperone mediated mechanisms (51). We examined the role of autophagy in the cellular trafficking of internalised aggregates using rapamycin. After incubation of cells with PepL, we did not observe any change in the uptake efficiency or the number or size of the intracellular compartments containing the peptides in rapamycin treated cells (Fig. 7A). To further study the role of autophagy, we assayed the internalisation of PepL in cells transduced with a GFP-LC3 expression vector that allows visualization of autophagosomes. The expression of this protein generated a cellular diffuse staining with the occasional presence of autophagosomes appearing as bright small vesicles (Fig. 7B, arrows). When cells expressing this GFP-LC3 protein were incubated with peptide PepL, no increase in the number of autophagosomes nor

colocalization between LC3 and the vesicles containing the peptides was detected (Fig. 7B). We therefore concluded that a role of autophagy in the processing of extracellular aggregates is unlikely.

Gene-expression analysis reveals a proteostatic response upon PepL uptake. The fact that KRIBB11 had an inhibitory effect on aggregate uptake suggests a proteostatic response of cells challenged by large aggregates. We analysed the cellular response to the presence of aggregates by mRNA microarray analysis at different time points of internalisation (8h and 24h after incubation). Changes in expression levels were evaluated using ANOVA with a significance threshold of $p<0.01$. Overall, PepL internalisation had a larger effect than PepS on the gene expression profile of HEK293 cells, both in terms of the number of affected genes (626 versus 377 after 24h) as on the magnitude of the changes (maximum fold change of 2.4 versus 1.5). Interestingly, there is only little overlap in gene-expression changes induced by PepS and PepL internalisation (4.5% after 8h, 4% after 24h). Looking at proteostatic changes in particular again confirmed a larger effect of PepL internalisation. Notably, we observed the upregulation of the Hsp70 family of chaperones and their co-chaperones of the Hsp40 family upon PepL but not PepS incubation (Fig. 7C). In accordance with this, we also observed the upregulation of the chaperone Hsp110 (HSPH1), that has been recently described as part of the cytosolic machinery responsible for the disaggregation of peptide aggregates (55–57). The other two main elements of the disaggregating complex, Hsp40 (DNAJA1) and Hsp70 (HSPA1A) were also upregulated in cells incubated with PepL (Fig. 7C). Many of these chaperones have been described as targets of HSF1 (Fig. 7C, highlighted). Although biologically relevant given the effect of HSF1 inhibition on aggregate uptake, the fold changes we found in response to aggregate uptake were low in comparison to the changes previously reported after heat shock and HSF1 activation, suggesting PepL internalisation induces a more subtle and less acute proteostatic response than thermal stress (58, 59).

Hsp70 inhibits PepL internalisation by blocking membrane interactions. To study the role of Hsp70 in aggregate uptake we first explored a possible extracellular activity of Hsp70. Preincubation of PepL with Hsp70 for 1h before adding it to the cells reduced the number of internalised aggregates to 20% after 24 hours of incubation (Fig. 8A). Importantly, the inhibitory effect could already be detected in the number of aggregates attached to the cell membranes within the first 2 hours of incubation (Fig. 8A, 2h). This decreased affinity for cell membranes is therefore the cause of the decreased internalisation. The subsequent trafficking of the aggregates after engulfment and their distribution to endolysosomes remained unaltered compared to control cells. This went along with a decreasing number of internalised aggregates after 48 h and an increasing number of endolysosomes as the result of aggregates being processed and targeted for lysosomal degradation (Fig. 8A). Importantly, the preincubation of PepL aggregates with Hsp70 inhibited their attachment and internalisation more efficiently than the simultaneous addition of aggregates and Hsp70 (Fig. 8A). This indicates that Hsp70 can alter the affinity of aggregates for the cell membrane by binding to areas on the aggregate that are required for their recognition, rather than by affecting cellular endocytic activity through the modulation of cell signalling pathways or the modification of components of the cell membrane. This view is confirmed by the co-immunoprecipitation of Hsp70 with pepL (Fig8E)

Although we observed a strong blockage of aggregate uptake by inhibiting the ATPase activity of Hsp70 with VER155008 (Fig. 7A), aggregate attachment was not affected by treatment with this inhibitor, since it did not decrease the number of PepL aggregates attached to cell membranes as compared to the untreated controls after 2 hours of incubation (Fig. 8B, upper panel). This implies that Hsp70 must be implicated in another step of peptide internalisation, for which Hsp70 chaperoning and ATPase activity are required. Blocking this step did not prevent the aggregates to attach to the membrane, since they remained associated and could be internalised upon removal of the inhibitor (Fig. 8B, upper panel, 24 and 48 hour time point). Comparably, membranes depleted of cholesterol by MβCD treatment showed the same affinity for PepL as the untreated controls (Fig. 8B, lower panel, 2h). Following MβCD removal, the subsequent uptake of the aggregates that were already attached to the

membrane was prevented by the continuous inhibition of cholesterol synthesis by mevanolin for 24h (Fig. 8B, lower panel). Removal of this inhibitor allowed the cells to restart peptide uptake after 24 h so these cells presented a similar amount of internalised aggregates to that of untreated controls (Fig. 8B, lower panel, 48 hour time point). This implies that cholesterol enriched lipid membrane rafts are not required for aggregate association to the membrane, though they may be important in the intracellular signalling leading to their internalisation.

To investigate why blocking PepL with soluble Hsp70 would impede recognition, we next tested whether membrane Hsp70 could be working as a receptor for the aggregates. We therefore blocked the extracellular exposed region of the membrane-inserted Hsp70 with a specific antibody (60). As shown in Figure 8C, a 1 hour preincubation of HEK-293 cells with this antibody did not prevent attachment, internalisation or processing of PepL aggregates in treated cells and resulted in a number of extracellular attached aggregates, internalised aggregates and endolysosomes comparable to the detected in untreated controls (Fig. 8C). In addition, we could not detect the presence of membrane Hsp70 in peptide-treated or control cells by confocal microscopy (Fig. 8D, right panels). By contrast, treatment of the cells with geldanamycin induced the translocation of Hsp70 to membrane patches resembling the previously described in the literature (61) (Fig. 8D, left panels). This result seems to rule out the possibility of direct interaction between Hsp70 and peptide aggregates on the cellular membrane.

DISCUSSION

We have described two pathways of entry of aggregating peptides in human cultured cells: fluid phase uptake of small aggregates and the internalisation of large aggregates by phagocytosis both of which are channelled into the endolysosomal system. Based on our experimental data, we propose that these two pathways occur by default in cells for the uptake of a given peptide in solution and are not mutually exclusive. Therefore a mixed solution containing both monomeric or oligomeric soluble peptide and large aggregates of several microns in diameter will be taken up by cells using both mechanisms. Importantly, the fluid phase uptake that we described is active for peptide whose sequences are not specifically attached to membranes. In cases where specific recognition of a peptide occurred, cells may use different endocytic mechanisms such as clathrin, caveolin or membrane translocation that would speed up their internalization with respect to this fluid phase uptake. Membrane association has been described previously in different models. For instance, charge dependent affinity for heparan sulfates is common in several cell penetrating peptides and amyloids (25, 34, 62). In the case of aggregating peptides, several amyloids have been proposed to be recognized by other membrane receptors, mostly of the TLR and scavenger families (26–31). Besides, it has been shown that amyloid conformation could determine membrane adhesion of small oligomers (63). Our results indicate that strongly aggregating peptides could reach a size that favours interaction with cell membranes regardless of their amyloid or amorphous organization, although the nature of this interaction remains to be investigated.

The internalisation of soluble amyloidogenic species has been previously described in cell culture for α-synuclein (15, 28) and both in cell culture and *in vivo* for Aβ (14, 24) either by specific uptake through receptor mediated endocytosis or passive diffusion across the cell membrane. In the case of Aβ, the internalisation of soluble species has been demonstrated to promote maturation into larger aggregates due to the acidic pH and increased concentration generated in the lysosomes. It is difficult to infer whether *in vivo* intracellular accumulation could be achieved only by unspecific intake during constitutive endocytosis. However, lysosomal accumulation of Aβ relies on a very slow rate of endocytosis together with a slow degradation rate (24), which are characteristics common to the mechanism described here. It is therefore possible that unspecific fluid phase endocytosis could contribute to the internalisation of aggregates *in vivo*.

Phagocytosis of extracellular aggregates by specialized cells is a documented feature of amyloid diseases. Microglia and astrocytes have been reported as fundamental in the clearance of Aβ plaques both *in vivo* and in cell culture (64, 65). Despite professional phagocytes being responsible for this function *in vivo*, it must be

considered that most of the non-professional phagocytic cell lines are capable of phagocytosis. Therefore it cannot be excluded that, in circumstances of increasing amyloid deposition in the extracellular space, non-professional phagocytic cell lines also internalise aggregated material, in the same way they do here when aggregates are directly decanted on their membranes in cell culture. In this regard, it must be considered that HEK-293 cells in our experiments required a minimum of 8h to complete engulfment of the phagocytized particles while Aβ-activated microglia can internalise microspheres in just 30 minutes (66). This is probably a reflection of the lack or low abundance of specific receptors in the cell membrane responsible for the recognition of the aggregating species such as Toll-like, scavenger, complement and Fc receptors.

PepL internalisation by phagocytosis is strongly decreased by chemical inhibition of Hsp70 function, which did not affect the internalisation of the smaller PepS aggregates by fluid phase internalisation. Moreover, exposure to the bigger basic PepL aggregates induced an upregulation of the Hsp70 expression level, while this remained unaffected in cells treated with the smaller acidic PepS aggregates. Both results argue in favour of a role for Hsp70 in the internalization of aggregates larger than 1 μm. Several possible functions of Hsp70 could explain these results. First, Hsp70 could be part of a chaperone-receptor complex on the cell membrane with adaptor roles between aggregate recognition and cell signalling. On the other hand, Hsp70 could be needed for its chaperoning action on components of the phagocytic machinery in an analogous way to its chaperone activity on clathrin (67). Finally, cytosolic Hsp70 could be regulating signal transduction pathways activated upon aggregate recognition. In any case, its function must be specific for aggregate recognition, since inhibition of Hsp70 activity did not alter the efficiency of the uptake of polystyrene beads. In this context, it must be as well considered that Hsp70 is part of the disaggregating complex formed together with Hsp40 and Hsp110 to promote disaggregation of intracellular aggregates. More importantly, the inhibition of Hsp70 activity with VER155008 halts the function of the whole disaggregating complex, so a possible dependency of aggregate uptake on disaggregase activity cannot be ruled out (55). It is relevant to point out that the morphological changes in the vesicles containing internalised aggregates, which are mostly vesicle growth to accommodate soluble material, are consistent with an intravesicular disaggregase activity. Regardless of the mechanism Hsp70 is implicated in, exposure to a high concentration of extracellular aggregates might sequester Hsp70 function, eliciting a compensatory chaperone response at the transcriptional level. This response is probably mediated by HSF1, since its specific chemical inhibition also partially inhibited aggregate uptake in our experiments.

Finally, several lines of work have demonstrated an important neuroprotective role for extracellular Hsp70 and other chaperones such as clusterin against the toxicity of several amyloids (68–70). This protective action has been attributed to the refolding and aggregation-inhibiting activity of the chaperone and to the activation of phagocytic cell types through membrane receptors to which Hsp70 binds directly (71, 72). In a complementary way, we have demonstrated here that extracellular Hsp70 can inhibit the interaction of peptide aggregates with cellular membranes without changing their aggregation status, which may have a large impact on the toxicity and extracellular clearance of aggregates from the intercellular space. In particular, as contact of extracellular Hsp70 with Toll-like receptors has been shown to activate phagocytosis by macrophages and microglia (71, 72), the inhibition of membrane interactions of aggregates with non-specialist cells might be an added advantage.

In conclusion, the results presented here show that cellular responses to extracellular aggregating peptides vary greatly depending on the biophysical properties of the aggregates including aggregation propensity and aggregate size and charge. While aggregates exceeding a diameter of a micron need specific membrane recognition and phagocytosis to enter the intracellular endosomal compartment of the cells, smaller aggregates are internalised unspecifically through fluid phase endocytosis. Importantly, large aggregates require aggregate-specific Hsp70 chaperone activity to be internalised and trigger a chaperone response in the cells. Further studies will be necessary to evaluate the actual role of Hsp70 in aggregate

recognition and uptake, which could represent a link for the transmission of extracellular proteostatic stresses into intracellular heat shock responses.

REFERENCES

1. Magalhães, A. C., Baron, G. S., Lee, K. S., Steele-Mortimer, O., Dorward, D., Prado, M. A. ., and Caughey, B. (2005) Uptake and neuritic transport of scrapie prion protein coincident with infection of neuronal cells. *J. Neurosci.* **25**, 5207–5216
2. Fevrier, B., Vilette, D., Archer, F., Loew, D., Faigle, W., Vidal, M., Laude, H., and Raposo, G. (2004) Cells release prions in association with exosomes. *Proc. Natl. Acad. Sci. U. S. A.* **101**, 9683–9688
3. Gousset, K., Schiff, E., Langevin, C., Marijanovic, Z., Caputo, A., Browman, D. T., Chenouard, N., de Chaumont, F., Martino, A., Enninga, J., Olivo-Marin, J.-C., Männel, D., and Zurzolo, C. (2009) Prions hijack tunnelling nanotubes for intercellular spread. *Nat. Cell Biol.* **11**, 328–336
4. Hofmann, J. P., Denner, P., Nussbaum-Krammer, C., Kuhn, P.-H., Suhre, M. H., Scheibel, T., Lichtenthaler, S. F., Schatzl, H. M., Bano, D., and Vorberg, I. M. (2013) Cell-to-cell propagation of infectious cytosolic protein aggregates. *Proc. Natl. Acad. Sci.* **110**, 5951–5956
5. Meyer-Luehmann, M., Coomaraswamy, J., Bolmont, T., Kaeser, S., Schaefer, C., Kilger, E., Neuenschwander, A., Abramowski, D., Frey, P., Jaton, A. L., Vigouret, J.-M., Paganetti, P., Walsh, D. M., Mathews, P. M., Ghiso, J., Staufenbiel, M., Walker, L. C., and Jucker, M. (2006) Exogenous Induction of Cerebral ß-Amyloidogenesis Is Governed by Agent and Host. *Science* **313**, 1781–1784
6. Frost, B., Jacks, R. L., and Diamond, M. I. (2009) Propagation of Tau Misfolding from the Outside to the Inside of a Cell. *J. Biol. Chem.* **284**, 12845–12852
7. Desplats, P., Lee, H.-J., Bae, E.-J., Patrick, C., Rockenstein, E., Crews, L., Spencer, B., Masliah, E., and Lee, S.-J. (2009) Inclusion formation and neuronal cell death through neuron-to-neuron transmission of α-synuclein. *Proc. Natl. Acad. Sci.* **106**, 13010–13015
8. Münch, C., O'Brien, J., and Bertolotti, A. (2011) Prion-like propagation of mutant superoxide dismutase-1 misfolding in neuronal cells. *Proc. Natl. Acad. Sci.* **108**, 3548–3553
9. Ren, P.-H., Lauckner, J. E., Kachirskaia, I., Heuser, J. E., Melki, R., and Kopito, R. R. (2009) Cytoplasmic penetration and persistent infection of mammalian cells by polyglutamine aggregates. *Nat. Cell Biol.* **11**, 219–225
10. Brundin, P., Melki, R., and Kopito, R. (2010) Prion-like transmission of protein aggregates in neurodegenerative diseases. *Nat. Rev. Mol. Cell Biol.* **11**, 301–307
11. Frost, B., and Diamond, M. I. (2010) Prion-like mechanisms in neurodegenerative diseases. *Nat. Rev. Neurosci.* **11**, 155–159
12. Goedert, M., Clavaguera, F., and Tolnay, M. (2010) The propagation of prion-like protein inclusions in neurodegenerative diseases. *Trends Neurosci.* **33**, 317–325
13. Omtri, R. S., Davidson, M. W., Arumugam, B., Poduslo, J. F., and Kandimalla, K. K. (2012) Differences in the Cellular Uptake and Intracellular Itineraries of Amyloid Beta Proteins 40 and 42: Ramifications for the Alzheimer's Drug Discovery. *Mol. Pharm.* **9**, 1887–1897
14. Kandimalla, K. K., Scott, O. G., Fulzele, S., Davidson, M. W., and Poduslo, J. F. (2009) Mechanism of Neuronal versus Endothelial Cell Uptake of Alzheimer's Disease Amyloid β Protein. *PLoS ONE* **4**, e4627
15. Lee, H.-J., Suk, J.-E., Bae, E.-J., Lee, J.-H., Paik, S. R., and Lee, S.-J. (2008) Assembly-dependent endocytosis and clearance of extracellular α-synuclein. *Int. J. Biochem. Cell Biol.* **40**, 1835–1849
16. Lee, S.-J., Desplats, P., Sigurdson, C., Tsigelny, I., and Masliah, E. (2010) Cell-to-cell transmission of non-prion protein aggregates. *Nat. Rev. Neurol.* **6**, 702–706
17. Rajendran, L., Honsho, M., Zahn, T. R., Keller, P., Geiger, K. D., Verkade, P., and Simons, K. (2006) Alzheimer's disease β-amyloid peptides are released in association with exosomes. *Proc. Natl. Acad. Sci.* **103**, 11172–11177

18. Emmanouilidou, E., Melachroinou, K., Roumeliotis, T., Garbis, S. D., Ntzouni, M., Margaritis, L. H., Stefanis, L., and Vekrellis, K. (2010) Cell-Produced α-Synuclein Is Secreted in a Calcium-Dependent Manner by Exosomes and Impacts Neuronal Survival. *J. Neurosci.* **30**, 6838–6851
19. Danzer, K. M., Kranich, L. R., Ruf, W. P., Cagsal-Getkin, O., Winslow, A. R., Zhu, L., Vanderburg, C. R., and McLean, P. J. (2012) Exosomal cell-to-cell transmission of alpha synuclein oligomers. *Mol. Neurodegener.* **7:42**
20. Alvarez-Erviti, L., Seow, Y., Schapira, A. H., Gardiner, C., Sargent, I. L., Wood, M. J. A., and Cooper, J. M. (2011) Lysosomal dysfunction increases exosome-mediated alpha-synuclein release and transmission. *Neurobiol. Dis.* **42**, 360–367
21. Vella, L., Sharples, R., Lawson, V., Masters, C., Cappai, R., and Hill, A. (2007) Packaging of prions into exosomes is associated with a novel pathway of PrP processing. *J. Pathol.* **211**, 582–590
22. Saman, S., Kim, W., Raya, M., Visnick, Y., Miro, S., Saman, S., Jackson, B., McKee, A. C., Alvarez, V. E., Lee, N. C. Y., and Hall, G. F. (2012) Exosome-associated Tau Is Secreted in Tauopathy Models and Is Selectively Phosphorylated in Cerebrospinal Fluid in Early Alzheimer Disease. *J. Biol. Chem.* **287**, 3842–3849
23. Pooler, A. M., Phillips, E. C., Lau, D. H. W., Noble, W., and Hanger, D. P. (2013) Physiological release of endogenous tau is stimulated by neuronal activity. *EMBO Rep.* **14**, 389–394
24. Hu, X., Crick, S. L., Bu, G., Frieden, C., Pappu, R. V., and Lee, J. M. (2009) Amyloid seeds formed by cellular uptake, concentration, and aggregation of the amyloid-beta peptide. *Proc. Natl. Acad. Sci.* **106**, 20324–20329
25. Kanekiyo, T., Zhang, J., Liu, Q., Liu, C.-C., Zhang, L., and Bu, G. (2011) Heparan Sulphate Proteoglycan and the Low-Density Lipoprotein Receptor-Related Protein 1 Constitute Major Pathways for Neuronal Amyloid-β Uptake. *J. Neurosci.* **31**, 1644–1651
26. Singh, T. D., Park, S.-Y., Bae, J., Yun, Y., Bae, Y.-C., Park, R.-W., and Kim, I.-S. (2010) MEGF10 functions as a receptor for the uptake of amyloid-β. *FEBS Lett.* **584**, 3936–3942
27. Sung, J. Y. (2001) Induction of Neuronal Cell Death by Rab5A-dependent Endocytosis of alpha - Synuclein. *J. Biol. Chem.* **276**, 27441–27448
28. Park, J.-Y., Kim, K. S., Lee, S.-B., Ryu, J.-S., Chung, K. C., Choo, Y.-K., Jou, I., Kim, J., and Park, S. M. (2009) On the mechanism of internalization of α-synuclein into microglia: roles of ganglioside GM1 and lipid raft. *J. Neurochem.* **110**, 400–411
29. Fellner, L., Irschick, R., Schanda, K., Reindl, M., Klimaschewski, L., Poewe, W., Wenning, G. K., and Stefanova, N. (2013) Toll-like receptor 4 is required for α-synuclein dependent activation of microglia and astroglia. *Glia* **61**, 349–360
30. Nakamura, K., Ohya, W., Funakoshi, H., Sakaguchi, G., Kato, A., Takeda, M., Kudo, T., and Nakamura, T. (2006) Possible role of scavenger receptor SRCL in the clearance of amyloid-βin Alzheimer's disease. *J. Neurosci. Res.* **84**, 874–890
31. Song, M., Jin, J., Lim, J.-E., Kou, J., Pattanayak, A., Rehman, J. A., Kim, H.-D., Tahara, K., Lalonde, R., and Fukuchi, K. (2011) TLR4 mutation reduces microglial activation, increases Aβ deposits and exacerbates cognitive deficits in a mouse model of Alzheimer's disease. *J. Neuroinflammation* **8:92**
32. Mandrekar, S., Jiang, Q., Lee, C. Y. D., Koenigsknecht-Talboo, J., Holtzman, D. M., and Landreth, G. E. (2009) Microglia Mediate the Clearance of Soluble Aβ through Fluid Phase Macropinocytosis. *J. Neurosci.* **29**, 4252–4262
33. Violetta, S., Maris, S. P., Thomas, L. W., Arjuna, R., Joe, A., Kirsti, G., Jack, T., Elisabeth, D., Roma, R., William, K., and others (2012) Visualization of co-localization in Abeta42-administered neuroblastoma cells reveals lysosome damage and autophagosome accumulation related to cell death. *Biochem. J.* **441**, 579–590

34. Horonchik, L., Tzaban, S., Ben-Zaken, O., Yedidia, Y., Rouvinski, A., Papy-Garcia, D., Barritault, D., Vlodavsky, I., and Taraboulos, A. (2005) Heparan Sulfate Is a Cellular Receptor for Purified Infectious Prions. *J. Biol. Chem.* **280**, 17062–17067
35. Kiachopoulos, S., Heske, J., Tatzelt, J., and Winklhofer, K. F. (2004) Misfolding of the Prion Protein at the Plasma Membrane Induces Endocytosis, Intracellular Retention and Degradation. *Traffic* **5**, 426–436
36. Luo, K., Li, S., Xie, M., Wu, D., Wang, W., Chen, R., Huang, L., Huang, T., Pang, D., and Xiao, G. (2010) Real-time visualization of prion transport in single live cells using quantum dots. *Biochem. Biophys. Res. Commun.* **394**, 493–497
37. Avrahami, D., Dayan-Amouyal, Y., Tal, S., Mincberg, M., Davis, C., Abramsky, O., and Gabizon, R. (2008) Virus-induced alterations of membrane lipids affect the incorporation of PrPSc into cells. *J. Neurosci. Res.* **86**, 2753–2762
38. Santa-Maria, I., Varghese, M., Księżak-Reding, H., Dzhun, A., Wang, J., and Pasinetti, G. M. (2012) Paired Helical Filaments from Alzheimer Disease Brain Induce Intracellular Accumulation of Tau Protein in Aggresomes. *J. Biol. Chem.* **287**, 20522–20533
39. Kfoury, N., Holmes, B. B., Jiang, H., Holtzman, D. M., and Diamond, M. I. (2012) Trans-cellular Propagation of Tau Aggregation by Fibrillar Species. *J. Biol. Chem.* **287**, 19440–19451
40. Bayer, T. A., and Wirths, O. (2010) Intracellular Accumulation of Amyloid-Beta - A Predictor for Synaptic Dysfunction and Neuron Loss in Alzheimer's Disease. *Front. Aging Neurosci.* **2:8**
41. LaFerla, F. M., Green, K. N., and Oddo, S. (2007) Intracellular amyloid-β in Alzheimer's disease. *Nat. Rev. Neurosci.* **8**, 499–509
42. Flannagan, R. S., Jaumouillé, V., and Grinstein, S. (2012) The Cell Biology of Phagocytosis. *Annu. Rev. Pathol. Mech. Dis.* **7**, 61–98
43. Irizarry, R. A., Hobbs, B., Collin, F., Beazer-Barclay, Y. D., Antonellis, K. J., Scherf, U., and Speed, T. P. (2003) Exploration, normalization, and summaries of high density oligonucleotide array probe level data. *Biostatistics* **4**, 249–264
44. Fernandez-Escamilla, A.-M., Rousseau, F., Schymkowitz, J., and Serrano, L. (2004) Prediction of sequence-dependent and mutational effects on the aggregation of peptides and proteins. *Nat. Biotechnol.* **22**, 1302–1306
45. Xu, J., Reumers, J., Couceiro, J. R., De Smet, F., Gallardo, R., Rudyak, S., Cornelis, A., Rozenski, J., Zwolinska, A., Marine, J.-C., Lambrechts, D., Suh, Y.-A., Rousseau, F., and Schymkowitz, J. (2011) Gain of function of mutant p53 by coaggregation with multiple tumor suppressors. *Nat. Chem. Biol.* **7**, 285–295
46. Otsuka, A., Abe, T., Watanabe, M., Yagisawa, H., Takei, K., and Yamada, H. (2009) Dynamin 2 is required for actin assembly in phagocytosis in Sertoli cells. *Biochem. Biophys. Res. Commun.* **378**, 478–482
47. Ivanov, A. I. (2008) Pharmacological inhibition of endocytic pathways: is it specific enough to be useful? *Methods Mol. Biol. Clifton NJ* **440**, 15–33
48. Nagao, G., Ishii, K., Hirota, K., Makino, K., and Terada, H. (2010) Role of Lipid Rafts in Phagocytic Uptake of Polystyrene Latex Microspheres by Macrophages. *Anticancer Res.* **30**, 3167–3176
49. Magenau, A., Benzing, C., Proschogo, N., Don, A. S., Hejazi, L., Karunakaran, D., Jessup, W., and Gaus, K. (2011) Phagocytosis of IgG-Coated Polystyrene Beads by Macrophages Induces and Requires High Membrane Order. *Traffic* **12**, 1730–1743
50. McClellan, A. J., Tam, S., Kaganovich, D., and Frydman, J. (2005) Protein quality control: chaperones culling corrupt conformations. *Nat. Cell Biol.* **7**, 736–741
51. Lamark, T., and Johansen, T. (2012) Aggrephagy: Selective Disposal of Protein Aggregates by Macroautophagy. *Int. J. Cell Biol.* **2012**, 1–21

52. Morimoto, R. I. (2008) Proteotoxic stress and inducible chaperone networks in neurodegenerative disease and aging. *Genes Dev.* **22**, 1427–1438
53. Åkerfelt, M., Morimoto, R. I., and Sistonen, L. (2010) Heat shock factors: integrators of cell stress, development and lifespan. *Nat. Rev. Mol. Cell Biol.* **11**, 545–555
54. Cortese, K., Howes, M. T., Lundmark, R., Tagliatti, E., Bagnato, P., Petrelli, A., Bono, M., McMahon, H. T., Parton, R. G., and Tacchetti, C. (2013) The HSP90 inhibitor geldanamycin perturbs endosomal structure and drives recycling ErbB2 and transferrin to modified MVBs/lysosomal compartments. *Mol. Biol. Cell* **24**, 129–144
55. Shorter, J. (2011) The Mammalian Disaggregase Machinery: Hsp110 Synergizes with Hsp70 and Hsp40 to Catalyze Protein Disaggregation and Reactivation in a Cell-Free System. *PLoS ONE* **6**, e26319
56. Rampelt, H., Kirstein-Miles, J., Nillegoda, N. B., Chi, K., Scholz, S. R., Morimoto, R. I., and Bukau, B. (2012) Metazoan Hsp70 machines use Hsp110 to power protein disaggregation. *EMBO J.* **31**, 4221–4235
57. Mattoo, R. U. H., Sharma, S. K., Priya, S., Finka, A., and Goloubinoff, P. (2013) Hsp110 is a bona fide chaperone using ATP to unfold stable misfolded polypeptides and reciprocally collaborate with Hsp70 to solubilize protein aggregates. *J. Biol. Chem.* **288**, 21399–21411
58. Trinklein, N. D., Murray, J. I., Hartman, S. J., Botstein, D., and Myers, R. M. (2004) The Role of Heat Shock Transcription Factor 1 in the Genome-wide Regulation of the Mammalian Heat Shock Response. *Mol. Biol. Cell* **15**, 1254–1261
59. Laramie, J. M., Chung, T. P., Brownstein, B., Stormo, G. D., and Cobb, J. P. (2008) Transcriptional profiles of human epithelial cells in response to heat: computational evidence for novel heat shock proteins. *Shock Augusta Ga* **29**, 623–630
60. Gehrmann, M., Marienhagen, J., Eichholtz-Wirth, H., Fritz, E., Ellwart, J., Jäättelä, M., Zilch, T., and Multhoff, G. (2005) Dual function of membrane-bound heat shock protein 70 (Hsp70), Bag-4, and Hsp40: protection against radiation-induced effects and target structure for natural killer cells. *Cell Death Differ.* **12**, 38–51
61. Vega, V. L., Rodríguez-Silva, M., Frey, T., Gehrmann, M., Diaz, J. C., Steinem, C., Multhoff, G., Arispe, N., and Maio, A. D. (2008) Hsp70 Translocates into the Plasma Membrane after Stress and Is Released into the Extracellular Environment in a Membrane-Associated Form that Activates Macrophages. *J. Immunol.* **180**, 4299–4307
62. Poon, G. M. K., and Gariépy, J. (2007) Cell-surface proteoglycans as molecular portals for cationic peptide and polymer entry into cells. *Biochem. Soc. Trans.* **35**, 788–793
63. Trevino, R. S., Lauckner, J. E., Sourigues, Y., Pearce, M. M., Bousset, L., Melki, R., and Kopito, R. R. (2012) Fibrillar Structure and Charge Determine the Interaction of Polyglutamine Protein Aggregates with the Cell Surface. *J. Biol. Chem.* **287**, 29722–29728
64. Lee, C. Y. D., and Landreth, G. E. (2010) The role of microglia in amyloid clearance from the AD brain. *J. Neural Transm.* **117**, 949–960
65. Paresce, D. M., Ghosh, R. N., and Maxfield, F. R. (1996) Microglial cells internalize aggregates of the Alzheimer's disease amyloid beta-protein via a scavenger receptor. *Neuron* **17**, 553–565
66. Koenigsknecht-Talboo, J., and Landreth, G. E. (2005) Microglial Phagocytosis Induced by Fibrillar β-Amyloid and IgGs Are Differentially Regulated by Proinflammatory Cytokines. *J. Neurosci.* **25**, 8240–8249
67. Sousa, R., and Lafer, E. M. (2006) Keep the Traffic Moving: Mechanism of the Hsp70 Motor. *Traffic* **7**, 1596–1603
68. Danzer, K. M., Ruf, W. P., Putcha, P., Joyner, D., Hashimoto, T., Glabe, C., Hyman, B. T., and McLean, P. J. (2011) Heat-shock protein 70 modulates toxic extracellular α-synuclein oligomers and rescues trans-synaptic toxicity. *FASEB J.* **25**, 326–336

69. Novoselova, T. V., Margulis, B. A., Novoselov, S. S., Sapozhnikov, A. M., Van Der Spuy, J., Cheetham, M. E., and Guzhova, I. V. (2005) Treatment with extracellular HSP70/HSC70 protein can reduce polyglutamine toxicity and aggregation. *J. Neurochem.* **94**, 597–606
70. Yerbury, J. J., and Wilson, M. R. (2010) Extracellular chaperones modulate the effects of Alzheimer's patient cerebrospinal fluid on Aβ1-42 toxicity and uptake. *Cell Stress Chaperones* **15**, 115–121
71. Kakimura, J.-I., Kitamura, Y., Takata, K., Umeki, M., Suzuki, S., Shibagaki, K., Taniguchi, T., Nomura, Y., Gebicke-Haerter, P. J., Smith, M. A., Perry, G., and Shimohama, S. (2002) Microglial activation and amyloid-beta clearance induced by exogenous heat-shock proteins. *FASEB J. Off. Publ. Fed. Am. Soc. Exp. Biol.* **16**, 601–603
72. Wang, R., Town, T., Gokarn, V., Flavell, R. A., and Chandawarkar, R. Y. (2006) HSP70 Enhances Macrophage Phagocytosis by Interaction With Lipid Raft-Associated TLR-7 and Upregulating p38 MAPK and PI3K Pathways. *J. Surg. Res.* **136**, 58–69

Acknowledgments. VIB Nucleomics Core (http://www.nucleomics.be) performed the microarray expression profile analysis. Bart de Strooper and Iryna Benilova for useful comments.

FOOTNOTES

*The Switch Laboratory and W.A. are supported by grants from VIB, University of Leuven (GOA/11/009 to W.A.), the Funds for Scientific Research Flanders (FWO), the Flanders Institute for Science and Technology (IWT) and the Federal Office for Scientific Affairs of Belgium (Belspo), IUAP P7/16 and the Hercules foundation (AKUL/09/037 and AKUL/11/30).

FIGURE LEGENDS

TABLE 1. Sequence, aggregation propensity and isoelectric point of the peptides used throughout this study. amino acids were coloured according to the properties of their side chains: blue, positively charge; red, negatively charged; green, aliphatic; grey, polar; purple, aromatic; orange, glycines; black, prolines. pI: isoelectric point.

FIGURE 1. Size analysis of PepL and PepS. A. Microscopic observation of the peptide solutions. Left panels. Electron microscopy. 20 µM solutions in PBS of FITC-conjugated peptides were negatively stained with uranyl acetate for TEM analysis. Scale bar: 1 µm. **Right panels. Confocal microscopy.** Peptides conjugated to Dylight#488 were resuspended in PBS to 20 µM and observed at the confocal microscope. Scale bar: 10 µm. **B. DLS analysis of the peptide solutions.** Size distribution of the aggregates present in 20 µM solutions in PBS of FITC-conjugated peptides were obtained by differential light scattering. The distributions were obtained by adjustment to a cumulant fit of the autocorrelation curves of 50 measurements of 5 s per sample. d: diameter.

FIGURE 2. Internalisation of PepL. A. Time lapse imaging of peptide aggregates in contact with cell membranes. HEK-293 cells were incubated in medium containing 20 µM PepL-Dylight#488 and observed *in vivo* at the confocal microscope. Peptide is shown in green over bright field images. **Upper panels.** Fragmentation of aggregate conglomerates and intercellular movement of aggregates. **Lower panels.** Aggregate movement from the periphery to perinuclear areas. A white dotted line was drawn around the nucleus for clarity. Scale bar: 10 µm. **B. Internalisation of PepL aggregates by confocal microscopy and TEM. Left panels:** HEK-293 cells were incubated in culture medium containing 20 µM PepL. At the indicated time points cells were fixed in glutaraldehyde and processed for TEM. Membrane interaction is shown in the upper panel (1 h), engulfment in the middle panel (8 h) and an "enlarged" vesicle is shown in the lower panel (24 h). Aggregated material is marked with an asterisk. Arrows indicate cellular protrusions. Nuclei are indicated with an "n". Scale: 1 µm. **Right panels.** HEK-293 cells were exposed to conglomerates of aggregates formed by Dylight#488 (green) and Dylight#550 (red) conjugated PepL (see text for details) and observed by confocal microscopy. Nuclei were stained with Hoechst (cyan). Scale bar: 10 µm. **C. Selective chemical inhibition of endocytic pathways.** HEK-293 cells were incubated in medium containing 5 µM PepL-Dylight#488 in the absence (mock) or presence of the indicated inhibitors at the following concentrations: 10 µM dynasore, 100 µM EIPA, 1 µM cytochalasin D, 10 mM MβCD followed by 10 µM mevinolin, 15 µM chlorpromazine. The number of cells containing internalised aggregates was quantified by high content analysis in vivo after 24h of incubation. The percentage of cells with aggregates with respect to the total was calculated for each condition and represented as the fold ratio with respect to untreated cells. Error bars represent the standard deviation of 3 independent experiments performed in duplicate. Statistical significance after ANOVA analysis with Tukey post-test indicated as follows: (●) $\alpha \leq 0.05$; (*) $\alpha \leq 0.01$; (**) $\alpha \leq 0.001$, (***) $\alpha = 0$.

FIGURE 3. Morphological analysis of enlarged vesicles. A. Photodisruption. A. A HEK-293 bearing an enlarged vesicle containing a PepL aggregate was illuminated constantly with the confocal laser (Argon 488 nm) for 15 min. Morphological changes in the vesicle were followed by time lapse confocal microscopy. **1)** 30 seconds. **2)** 3 min **3)** 9 min **4)** 13 min **5)** 14 min. **6)** 15 min. **B. Fixation artefacts.** HEK-293 cells were incubated for 24 h with PepL-Dylight#488 aggregates and imaged by: bright field microscopy *in vivo* **(1)**,bright field after fixation in 4% formaldehyde for 20 min **(2)** and confocal microscopy after fixation in 4% formaldehyde **(3)** or 2.5% glutaraldehyde**(4)** followed by permeabilization in 0.1% Triton X-100. Green: PepL, Red: autofluorescence. Enlarged vesicles are indicated by arrows. Scale bar: 10 µm.

FIGURE 4. Endocytic pathways of peptide PepL internalisation. A. Endocytic markers. HEK-293 cells expressing the RFP-fusion proteins (red) indicated were incubated in medium containing 20 µM PepL-Dylight#488 (green). The internalisation process was followed by life confocal imaging at the indicated time points. **B. Early endosome function inhibition.** Cells expressing the constitutively active mutant $Rab5^{Q79L}$ were incubated in culture medium containing 20 µM PepL-Dylight#488 and imaged as in A. Scale bar for A. and B.: 10 µm.

FIGURE 5. Endocytic pathways of peptide PepS internalisation. A. Dextran10 co-incubation. HEK-cells were incubated in medium containing 20 µM Dextran10-TexasRed (red) in the presence or absence of 20 µM PepS-Dylight#488 (green). The internalisation process was followed by life confocal imaging at the indicated time points. Medium was removed just before imaging at each time point to remove background fluorescence. Scale bar: 20 µm. **B. Selective chemical inhibition of endocytic pathways.** HEK-293 cells were incubated in medium containing 5 µM PepS-Dylight#488 in the absence (mock) or presence of the indicated inhibitors at the concentrations indicated in Fig. 2C. The number of fluorescent vesicles per cell after 24h of incubation was quantified by high content analysis *in vivo* and represented as the fold ratio with respect to untreated cells. Error bars represent the standard deviation of 3 independent experiments performed in duplicate. Statistical significance indicated as in Fig. 2C: (●) $\alpha \leq 0.05$; (*) $\alpha \leq 0.01$; (**) $\alpha \leq 0.001$, (***) $\alpha = 0$. **C. Endocytic markers.** Cells expressing the indicated RFP-fusion proteins (red) were incubated in medium containing 20 µM PepS-Dylight#488 and imaged at the indicated time points by *in vivo* confocal microscopy. Scale bar: 20 µm.

FIGURE 6. Internalization of peptides Inf12 and Inf36. HEK-293 cells were incubated in medium containing 5 µM concentrations of peptides Inf12-Dylight#488 or Inf36-Dylight#488. The internalization was followed by *in vivo* confocal microscopy. Images were taken at the indicated time points. Arrows: intracellular inclusions. Scale bar: 10 µm

FIGURE 7. Role of the protein quality control system in the internalisation of aggregating peptides. A. Selective chemical inhibition of various agents of the protein quality control system. HEK-293 cells were incubated in medium containing 5 µM concentrations of peptides PepL-Dylight#488 or PepS-Dylight#488 or in a 1% suspension of polystyrene microspheres (3 µm diameter Fluoresbrite Microparticles -Polysciences, Inc-) in the absence (mock) or presence of the following inhibitors: 10 µM KRIBB11, 40 µM VER155008, 10 µM geldanamycin, 100 nM rapamycin and 1 µM cytochalasin D. Different quantifications of size and number of the different vesicle types and beads were performed by high content analysis *in vivo* after 24h of incubation. Error bars represent the standard deviation of 3 independent experiments performed in duplicate. Statistical significance indicated as for Fig. 2C: (●) $\alpha \leq 0.05$; (*) $\alpha \leq 0.01$; (**) $\alpha \leq 0.001$, (***) $\alpha = 0$. **B. LC3 localization.** HEK-293 cells expressing a fluorescent fusion protein GFP-LC3 (green) were incubated in medium containing 5 µM PepL-Dylight#550 (red) and analysed by *in vivo* confocal microscopy. Images were captured after an overnight incubation. **C. Expression levels of several representative members of the quality control system after incubation with aggregating peptides.** HEK-293 cells were incubated for 24h in medium containing 5 µM PepL or PepS. Cells were then lysed and total mRNAs were extracted, purified and hybridized in an expression profile microarray (Affymetrix Human PrimeView). Green bars indicate

upregulated genes and red bars downregulated genes for each of the peptides. Expression levels are the average of three independent experimental replicates and are represented as the fold change with respect to untreated controls.

FIGURE 8. Role of Hsp70 in the internalisation of PepL aggregates. A. Extracellular addition of Hsp70 protein. A mixed solution of 6 μM PepL and 1.2 μM Hsp70 in PBS was incubated at 37°C for 1h and then added to the culture medium of HEK-293 cells at a 90% confluency to a final concentration of 2 μM PepL and 400 nM Hsp70 (green bars, "preincubation"). Alternatively, a PepL/Hsp70 solution at the same concentration was added to cells without any previous incubation (red bars, "simultaneous addition"). As a negative control, a solution containing only 6 μM PepL was added to the cell culture medium (blue bars, "mock"). To measure the amount of peptide attached to the cell membranes, the solution containing the peptide was removed after 1h incubation and cells were washed twice with complete medium. The number of aggregates remained attached to cell membranes was then quantified by high content analysis (time point "2h"). 24 and 48 hours after peptide addition, the number of internalised aggregates (upper panel) and endolysosomes (lower panel) was also quantified by high content analysis. A dotted vertical grey line separates the time points where extracellular aggregates were quantified from time points showing intracellular aggregates. **B. Effect of Hsp70 inhibition and cholesterol depletion on aggregate membrane attachment.** HEK-293 cells were incubated in medium containing 5 μM PepL-Dylight#488 in the absence (mock) or presence of the indicated inhibitors. Upper panel: after a 1 hour incubation in the absence or presence of 40 μM VER155008, medium was removed and cells were washed twice in complete cell culture medium and incubated without inhibitor for the indicated time periods. Lower Panel: after a 1h incubation in 10 mM MβCD cells were washed twice in complete medium and incubated in medium containing 10 μM mevinolin ("MβCD/Mevinolin") or in the absence of inhibitors ("Mock" and "MβCD"). After additional 24 hours, mevinolin was removed by two medium washes and cells were incubated for 24h more (48h time point). The number of attached extracellular and internalised aggregates was quantified as indicated in section A. **C. Hsp70 blocking antibodies.** cmHsp70.1 antibody was diluted in the culture medium of HEK-293 cells to the indicated concentrations and incubated for 1 hour. A solution of PepL was then added to the culture medium to a final concentration of 5 μM. After a 1 hour incubation, medium was removed and cells were washed twice and incubated in complete cell culture medium for the indicated time points. The number of attached extracellular and internalised aggregates was quantified as indicated in section A. **D. Membrane Hsp70 staining.** HEK-293 cells were either treated with 10 μM geldanamycin or 5 μM peptide PepL-Dylight#550 (red) or left untreated. After an overnight incubation cells were stained for immunofluorescence with antibody cmHsp70.1-Cy2 (green) and fixed. In samples incubated with aggregates, peptide autofluorescence is responsible for the green signal observed in both antibody-treated and untreated cells samples. Scale bar: 20 μm.

Table 1

Peptide	Sequence	Tango score	pI
PepL	RPILTIITLERGSRRPILTIITLE	1273.17	11.52
PepS	DMISYAGMDPPDMISYAGMD	10.44	3.32
Inf12	RLIQLIVSRPPRLIQLIVSR	532.08	12.48
Inf36	RGVSILNLRPPRGVSILNLR	29.36	12.48

Figure 1

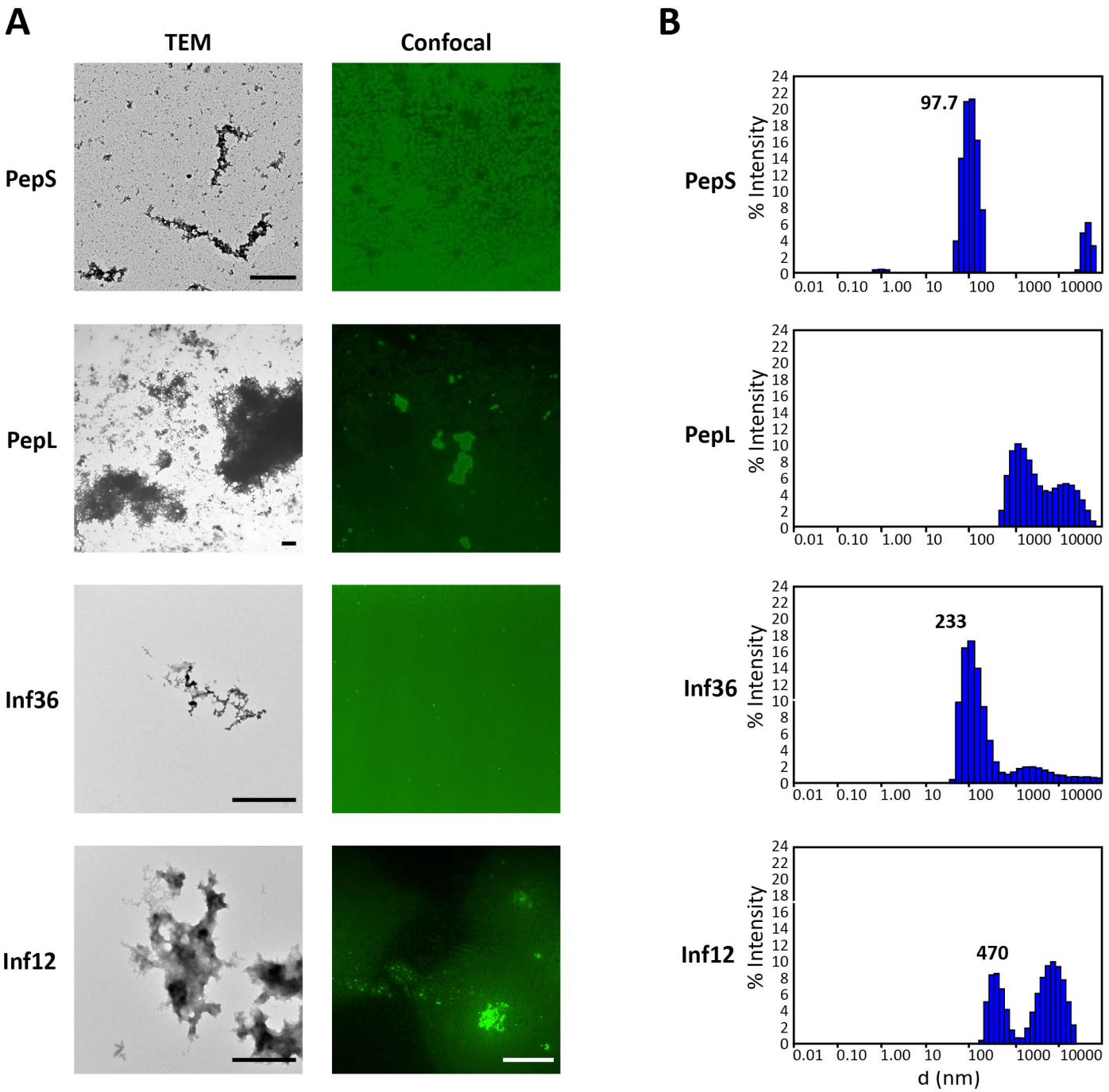
A
TEM
Confocal
PepS
PepL
Inf36
Inf12
B
PepS
PepL
Inf36
Inf12
% Intensity
97.7
233
470
0.01
0.10
1.00
10
100
1000
10000
d (nm)

Figure 2

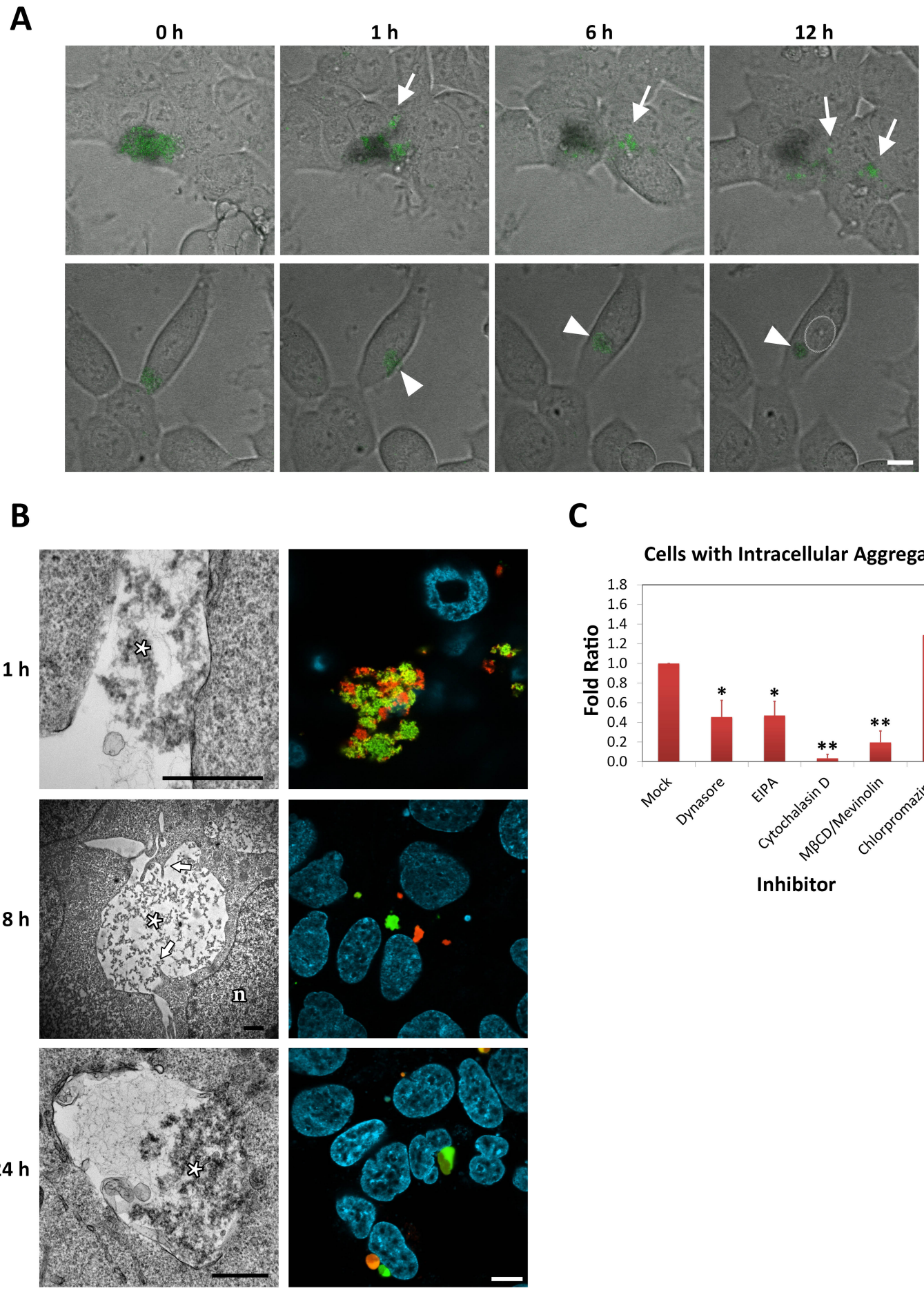
A
0 h
1 h
6 h
12 h
B
1 h
8 h
24 h
n
C
Cells with Intracellular Aggregates
Fold Ratio
1.8
1.6
1.4
1.2
1.0
0.8
0.6
0.4
0.2
0.0
*
*
**
**
Mock
Dynasore
EIPA
Cytochalasin D
MβCD/Mevinolin
Chlorpromazine
Inhibitor

Figure 3

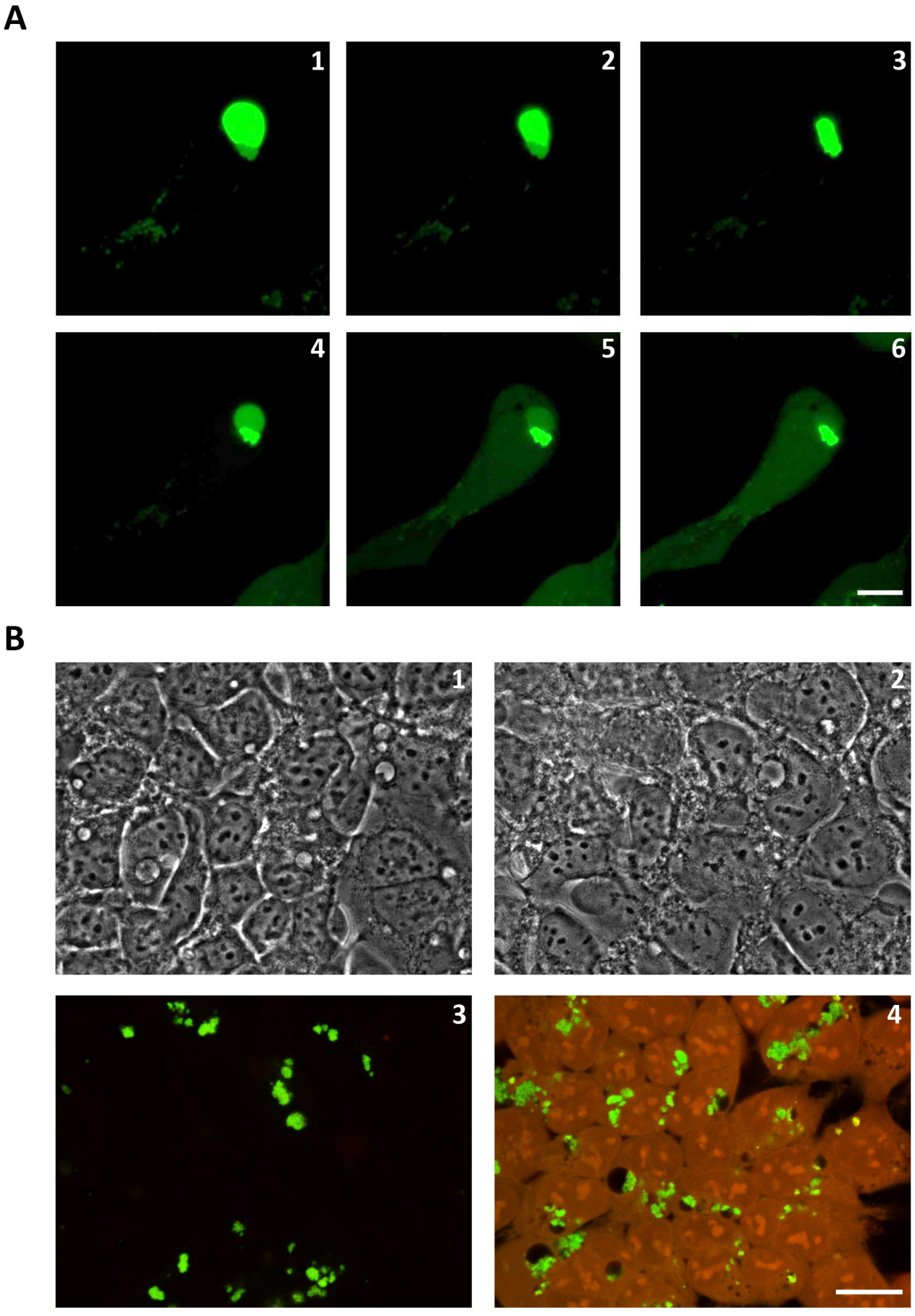

Figure 4

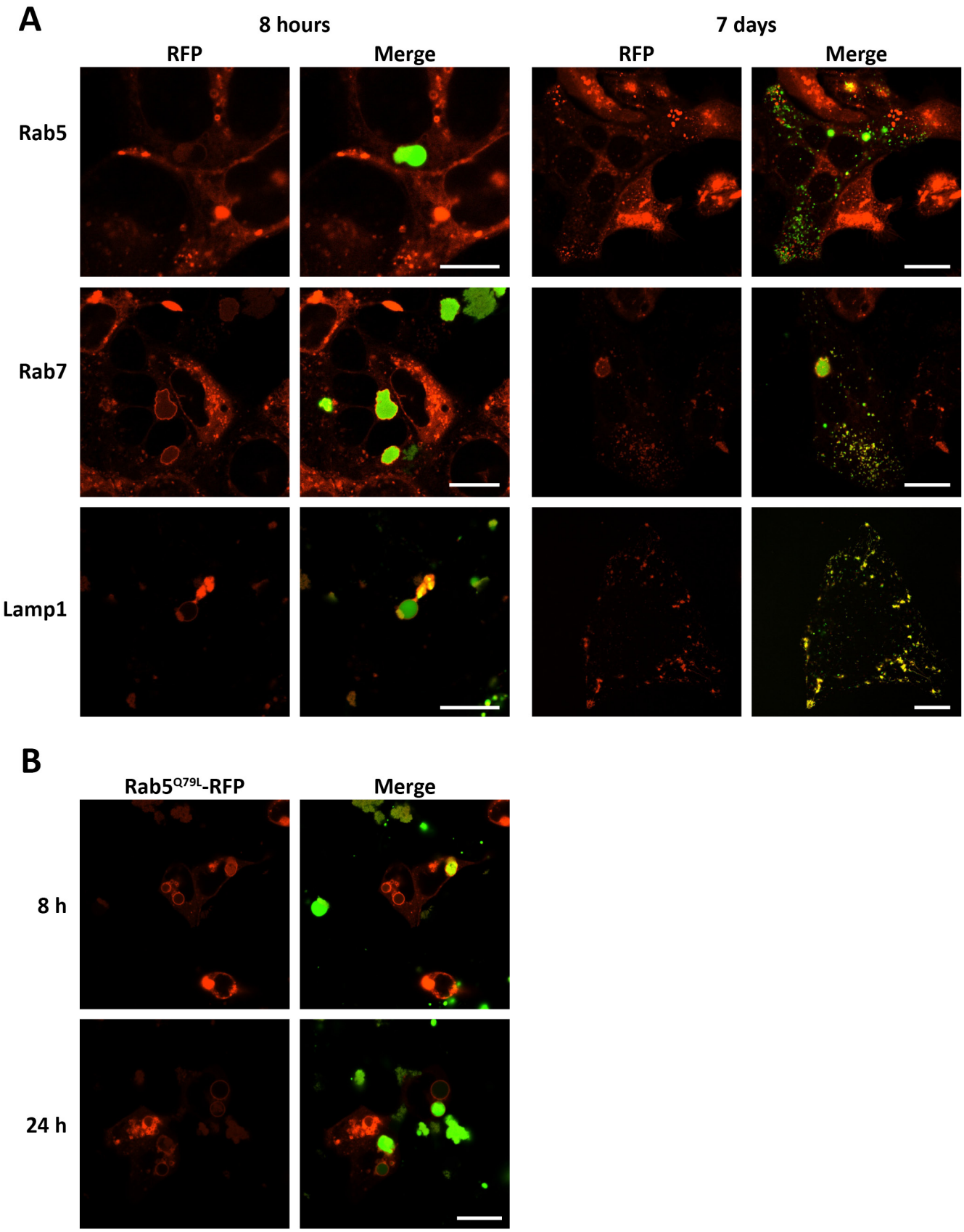
A
8 hours
7 days
RFP
Merge
RFP
Merge
Rab5
Rab7
Lamp1
B
Rab5Q79L-RFP
Merge
8 h
24 h

Figure 5

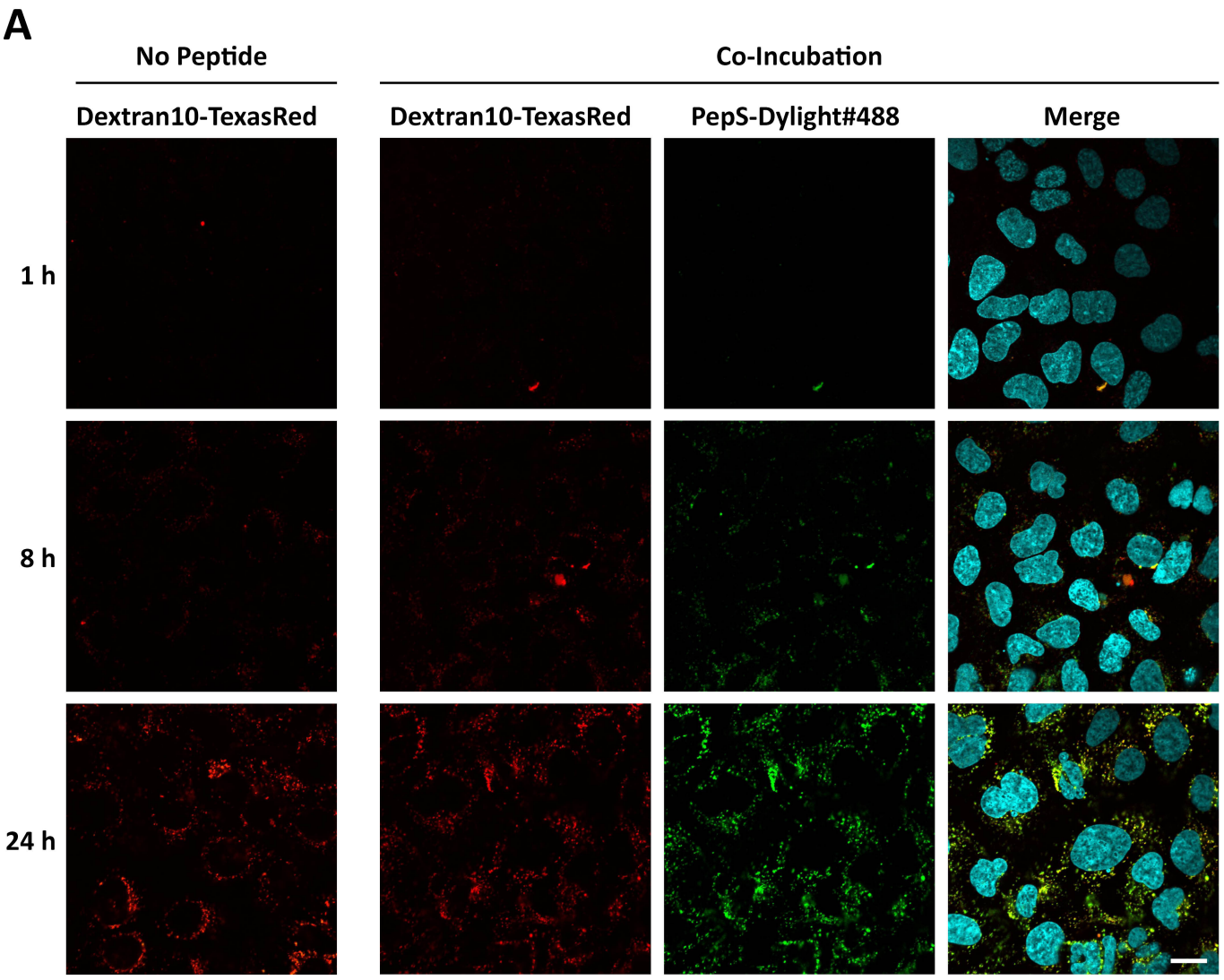
A
No Peptide
Co-Incubation
Dextran10-TexasRed
Dextran10-TexasRed
PepS-Dylight#488
Merge
1 h
8 h
24 h

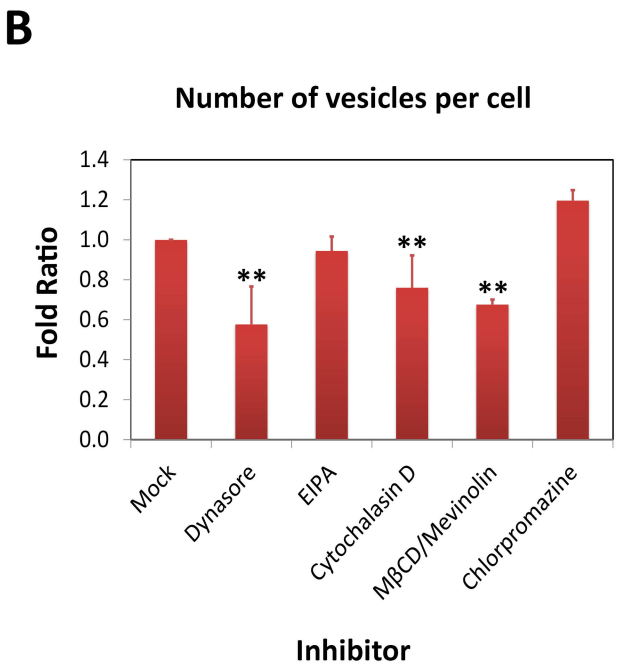
B
Number of vesicles per cell
Fold Ratio
1.4
1.2
1.0
0.8
0.6
0.4
0.2
0.0
**
**
**
Mock
Dynasore
EIPA
Cytochalasin D
MβCD/Mevinolin
Chlorpromazine
Inhibitor

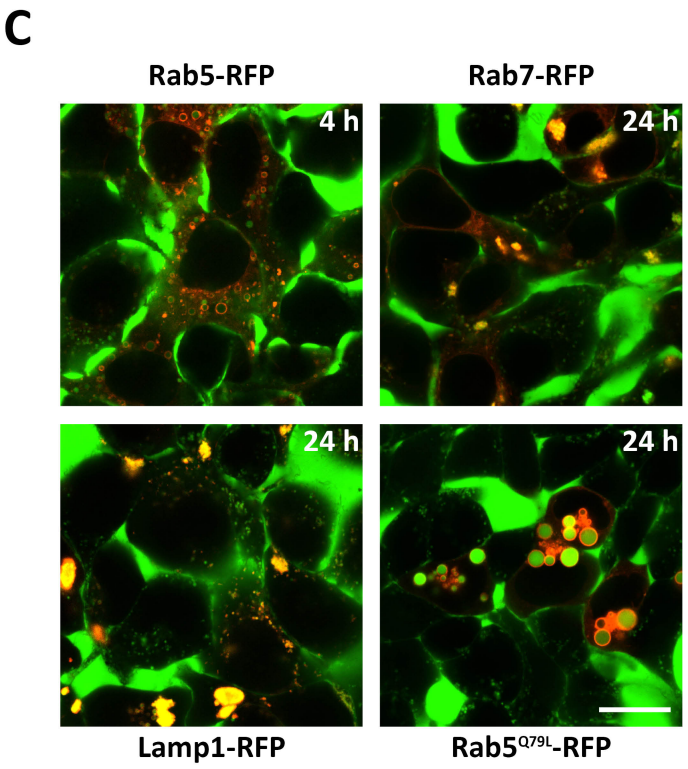
C
Rab5-RFP
Rab7-RFP
4 h
24 h
24 h
24 h
Lamp1-RFP
Rab5Q79L-RFP

Figure 6

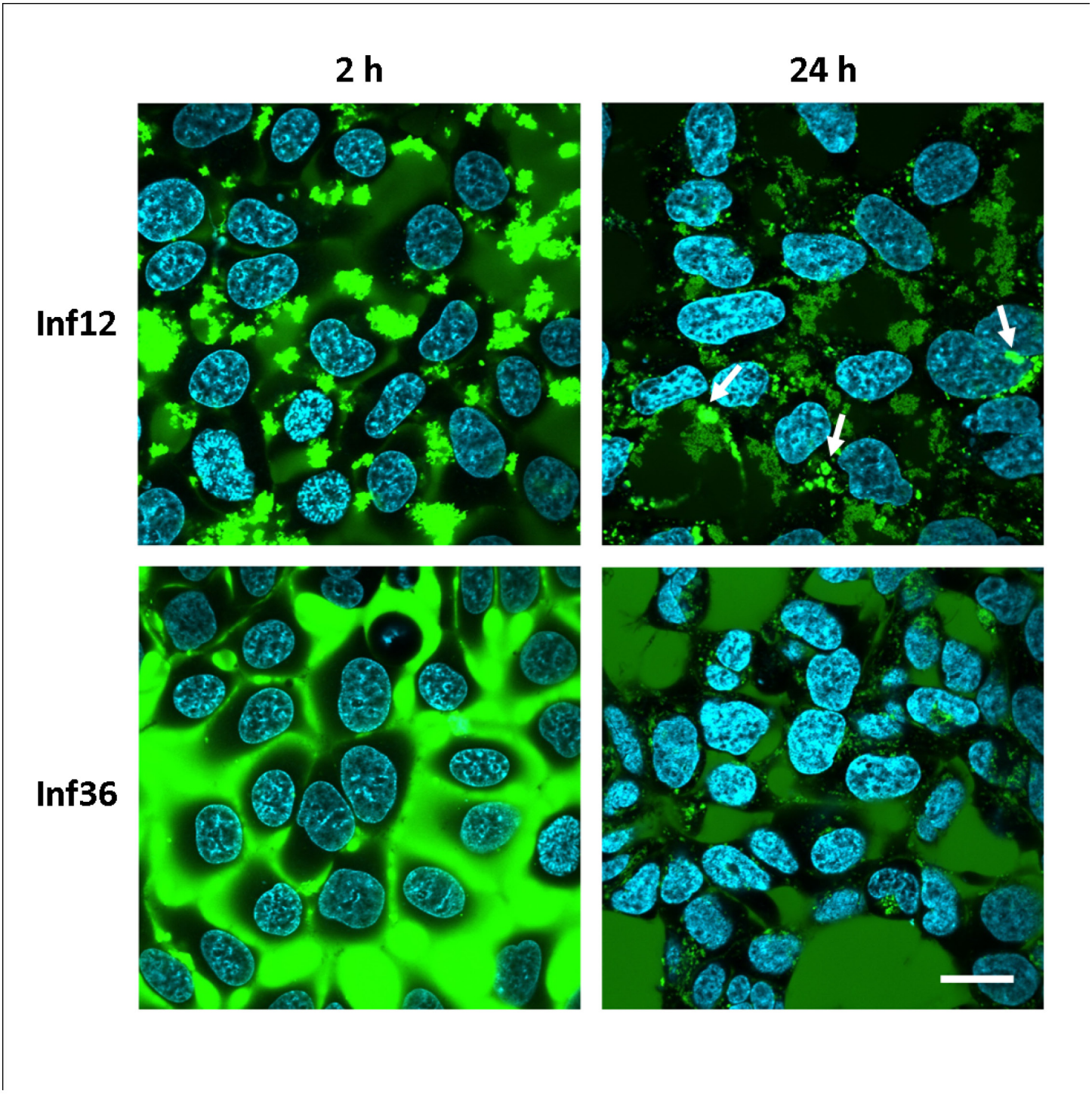

Figure 7

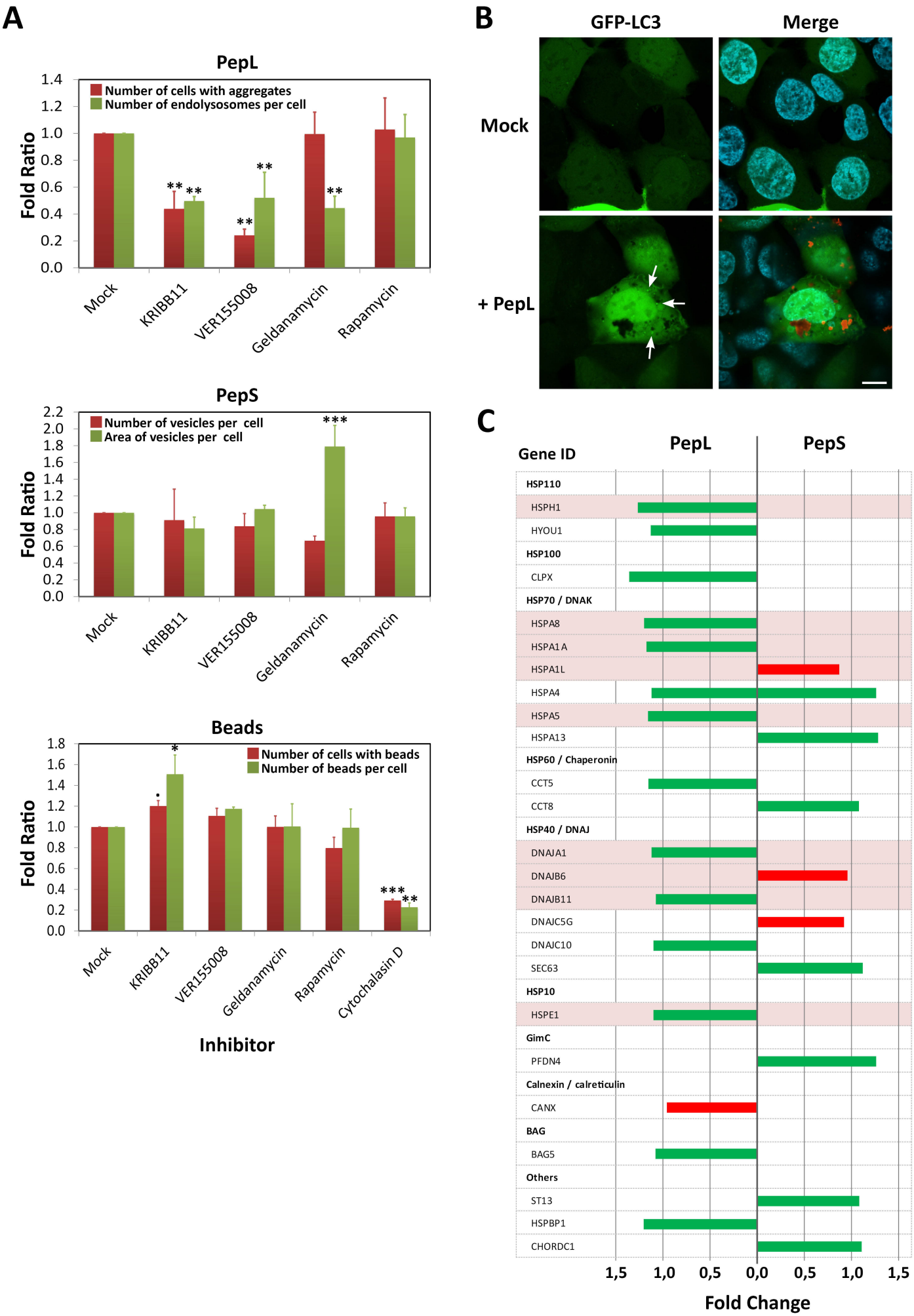
A
PepL
Number of cells with aggregates
Number of endolysosomes per cell
Fold Ratio
Mock
KRIBB11
VER155008
Geldanamycin
Rapamycin
PepS
Number of vesicles per cell
Area of vesicles per cell
Beads
Number of cells with beads
Number of beads per cell
Cytochalasin D
Inhibitor
B
GFP-LC3
Merge
Mock
+ PepL
C
Gene ID
PepL
PepS
HSP110
HSPH1
HYOU1
HSP100
CLPX
HSP70 / DNAK
HSPA8
HSPA1A
HSPA1L
HSPA4
HSPA5
HSPA13
HSP60 / Chaperonin
CCT5
CCT8
HSP40 / DNAJ
DNAJA1
DNAJB6
DNAJB11
DNAJC5G
DNAJC10
SEC63
HSP10
HSPE1
GimC
PFDN4
Calnexin / calreticulin
CANX
BAG
BAG5
Others
ST13
HSPBP1
CHORDC1
Fold Change

Figure 8

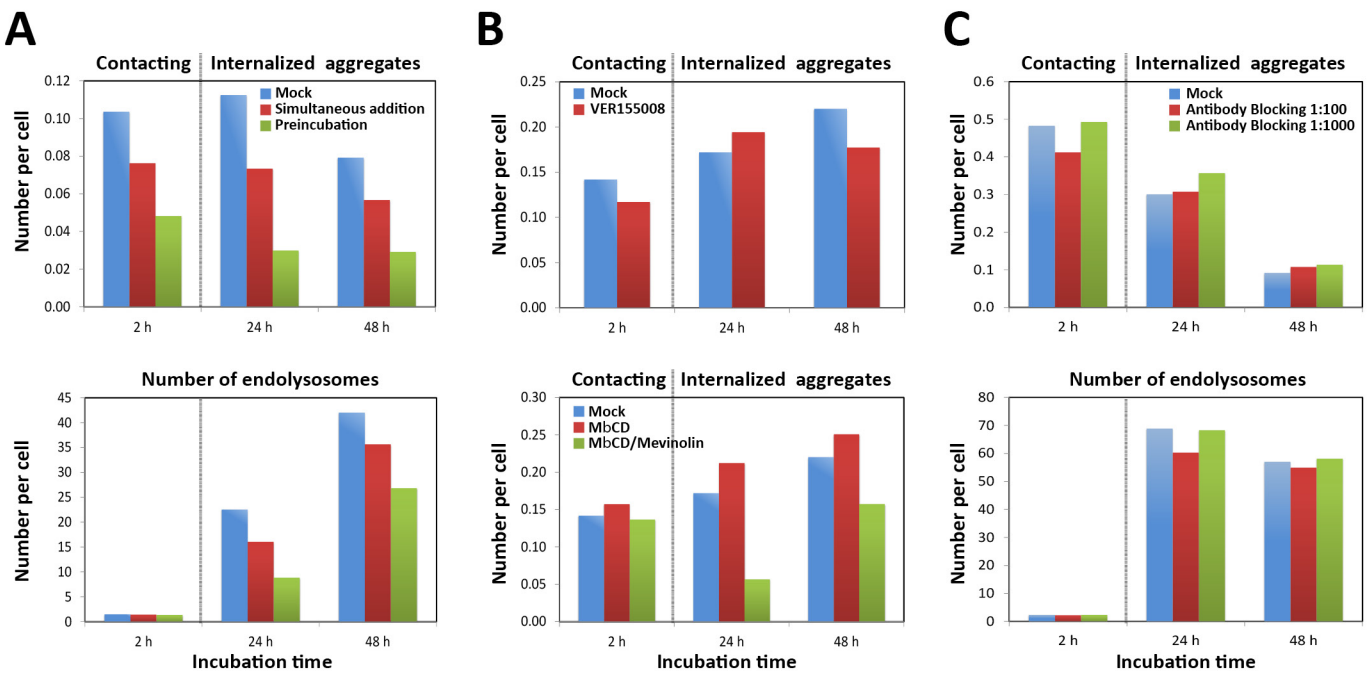
A
Contacting
Internalized aggregates
Number per cell
Mock
Simultaneous addition
Preincubation
2 h
24 h
48 h
Number of endolysosomes
Incubation time
B
Contacting
Internalized aggregates
Number per cell
Mock
VER155008
Contacting
Internalized aggregates
Mock
MbCD
MbCD/Mevinolin
Incubation time
C
Contacting
Internalized aggregates
Number per cell
Mock
Antibody Blocking 1:100
Antibody Blocking 1:1000
Number of endolysosomes
Incubation time

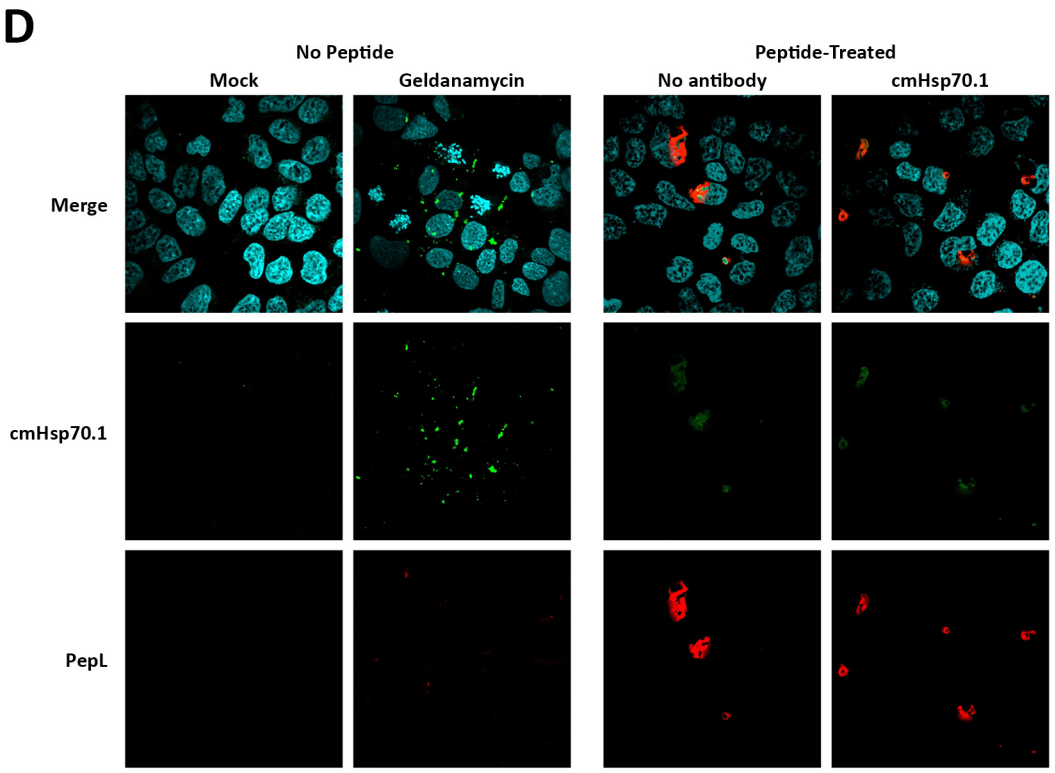
D
No Peptide
Peptide-Treated
Mock
Geldanamycin
No antibody
cmHsp70.1
Merge
cmHsp70.1
PepL

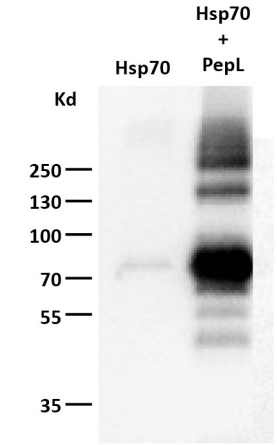
E
Hsp70
Hsp70 + PepL
Kd
250
130
100
70
55
35